# Transport Properties in Carbon Nanotubes

**Stefano Bellucci and Pasquale Onorato**

**Abstract** This chapter focuses on the general theory of the electron transport properties of carbon nanotubes, yielding an overview of theoretical models. It is organized in five sections describing the results of the research activity performed in electronic/electrical properties modelling. The first section, in addition to describing the scope of the review and providing an introduction to its content, yields as well a general introduction on carbon nanotubes. Sect. 'Electronic Structure of Single-Wall Nanotubes' describes the general theory of the electron transport in carbon nanotubes, starting from the band structure of graphene. Sect. 'Quantum Transport in Carbon Nanotubes' focuses on the quantum transport in carbon nanotubes, including ballistic transport, Coulomb-blockade regime, Luttinger Liquid theory. Sect. 'Results and Experiments' reports results and experimental evidence of the models decribed. Finally, Sect. 'Superconducting transition' addresses the issue of superconductivity transitions in carbon nanotubes.

## Introduction

In the last 20 years progresses in technology allowed for the *construction* of several new devices in the range of nanometric dimensions. The well known Moore prediction states that the silicon-data density on a chip doubles every 18 months. So we are going toward a new age when the devices in a computer will live on the nanometer scale and will be ruled by the Quantum Mechanics laws.

Recently several scientists proposed a new carbon based technology against the usual silicon one. The allotropes of carbon, carbon nanotubes, single atomic layers of graphite (graphene), fullerene molecules and diamond have emerged recently as new electronic materials with unique properties. In this sense the discovery of

S. Bellucci (✉)
INFN, Laboratori Nazionali di Frascati, P.O. Box 13, 00044 Frascati, Italy
e-mail: stefano.bellucci@lnf.infn.it

S. Bellucci (ed.), *Physical Properties of Ceramic and Carbon Nanoscale Structures*,
Lecture Notes in Nanoscale Science and Technology 11,
DOI 10.1007/978-3-642-15778-3_2, 

carbon nanotubes in 1991 [1] opened a new field of research in the physics at nanoscales [2]. Thus carbon nanotubes have become very promising in the field of molecular electronics, in which atoms and molecules are envisaged as the building blocks in the fabrication of electronic devices.

## *Hystory and Structure*

The existence of single-walled carbon tubes was pointed out in 1976 [3] but the subject seems to have become prominent after the discovery of fullerene in 1985 [4] and the identification of nanotubes by Iijima in 1991 [1].

Carbon nanotubes (CNs) are basically rolled up sheets of graphite (hexagonal networks of carbon atoms) forming tubes that are only nanometers in diameter and have length up to some microns (see Fig. 1. *top*). Several experiments in the last 15 years have shown their interesting properties [5–7]. The nanometric size of CNs, together with the unique electronic structure of a graphene sheet, make the electronic prop erties of these one-dimensional (1D) structures highly unusual.

CNs may also display different behaviors depending on whether they are single-walled carbon nanotubes (SWNTs) or multi-walled carbon nanotubes (MWNTs) that are typically made of several (typically 10) concentrically arranged graphene sheets (see Fig. 1. *left bottom*). Thus SWNT can be thought of as the fundamental cylindrical structure, and these form the building blocks of both multi-wall nanotubes and the arrays of single-wall nanotubes, also bundles. Bundles typically contain many tens of nanotubes and can be considerably longer and wider than the nanotubes from which they are formed. This could have important toxicological

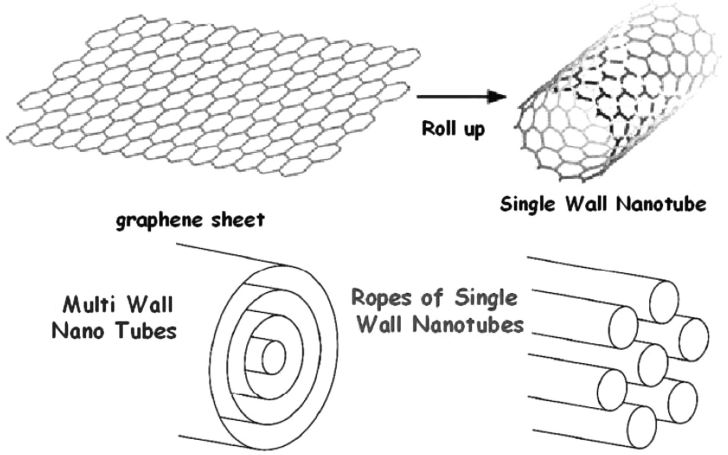


**Fig. 1** The structure of a SWNT can be conceptualized by wrapping a one-atom-thick layer of graphite called graphene into a seamless cylinder. The way the graphene sheet is wrapped is represented by a pair of indices (n,m) called the chiral vector. The integers n and m denote the number of unit vectors along two directions in the honeycomb crystal lattice of graphene. (*Bottom left*) Multi Wall Nano Tubes : several (typically 10) concentrically arranged graphene sheets (Russian doll) (*Bottom right*) Ropes of SWCNTs Triangular lattice of 5–100 SWCNT

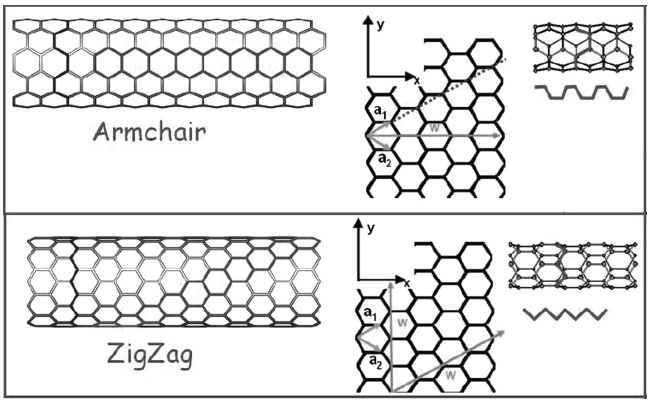


**Fig. 2** Armchair and ZigZag nanotubes. The CN is made by coiling a graphene sheet about two points connected by the vector $\vec{w}$. (*Top*) In the case of armchair the vector $\vec{w}$ is known as $\vec{w} = (n \cdot a_1) + (n \cdot a_2)$, or $\vec{w} = (n, n)$. (*Bottom*) The second nanotube, the ZigZag one, is made by coiling a graphene sheet with a vector $(n \cdot a_1) + (0 \cdot a_2)$, or $(n, 0)$. Notice that analogous ZigZag CN is obtained with a wrapping vector $(n, -n)$

consequences. The strong tendency of both SWCNT or MWCNT to bundle together in ropes is a consequence of attractive van der Waals forces analogous to forces that bind sheets of graphite [8]. In Ref. [8] the authors found that the individual SWNTs are packed into a close-packed triangular lattice with a lattice constant of about 17 Å the density, lattice parameter, and interlayer spacing of the ropes was dependent on the chirality of the tubes in the mat [9] (see Fig. 2).

## *Synthesis and Characterization*

CNs vary significantly in length and diameter depending on the synthetic procedure. Lengths are generally dependent on synthesis time but are typically tens of microns, although significantly shorter and longer nanotubes have been made [10, 11]. An individual SWNT has typical dimensions $L : 1\,\mu\text{m}$ and $R : 1\,\text{nm}$ while MWCNT generally range from 10 nm to 200 nm in diameter [12].

## *Structure of a Single Wall CN*

A few key studies have explored the structure of carbon nanotubes using high-resolution microscopy techniques. These experiments have confirmed that nanotubes are cylindrical structures based on the hexagonal lattice of carbon atoms that forms crystalline graphite.

Three types of nanotubes are possible, called armchair, zigzag and chiral nanotubes, depending on how the two-dimensional graphene sheet is 'rolled up' (see

Fig. 1). The different types are most easily explained in terms of the unit cell of a carbon nanotube, the smallest group of atoms that defines its structure [13].

There are many ways of choosing the lattice vectors, but some are more comfortable to work with than others. In Fig. 1 we have chosen $a_1$ and $a_2$ to be two upright secants of a isosceles triangle within two hexagons. In Cartesian coordinates the lattice vectors can be written as,

$$a_1 = \frac{a_0}{2}(3, \sqrt{3}) = \frac{a}{2}(\sqrt{3}, 1), \quad a_2 = \frac{a_0}{2}(3, -\sqrt{3}) = \frac{a}{2}(\sqrt{3}, -1)$$

where $a_0 \approx 1.42$Å is the carbon-carbon distance and $a = \sqrt{3}a_0$. The so-called chiral (or wrapping) vector of the nanotube, $\vec{w}$, is defined by

$$\vec{w} = m_w a_1 + n_w a_2,$$

where $n_w$ and $m_w$ are integers. The roll up vector, $\vec{w}$, (also called the Chiral vector $\vec{C}_h$) determines the circumference of the carbon nanotube. In fact the radius, $R$, is simply the length of the chiral vector divided by $2\pi$, and we find that

$$R = \frac{|(m_w \cdot a_1) + (n_w \cdot a_2)|}{2\pi}.$$

Another important parameter is the chiral angle, which is the angle between $\vec{w}$ and $a_1$. When the graphene sheet is rolled up to form the cylindrical part of the nanotube, the ends of the chiral vector meet each other. The chiral vector thus forms the circumference of the nanotube's circular cross-section, and different values of n and m lead to different nanotube structures. Armchair nanotubes are formed when $n_w = m_w$ and the chiral angle is 30° (see *top* figure). Zigzag nanotubes are formed when either n or m are zero and the chiral angle is 0°. All other nanotubes, with chiral angles intermediate between 0° and 30°, are known as chiral nanotubes. The properties of nanotubes are determined by their diameter and chiral angle, both of which depend on $\vec{w}$.

Thus values of $n_w$ and $m_w$ determine the chirality, or 'twist' of the nanotube. The chirality in turn affects the conductance of the nanotube, its density, its lattice structure, and other properties. As we demonstrate below SWNT is considered metallic if the value $n_w - m_w$ is divisible by three. Otherwise, the nanotube is semiconducting. Consequently, when tubes are formed with random values of $n_w$ and $m_w$, we would expect that two-thirds of nanotubes would be semi-conducting, while the other one-third would be metallic, which happens to be the case.

## Electronic Structure of Single-Wall Nanotubes

As we discussed above the electronic properties of CNs depend on their diameter, chiral angle (helicity) parameterized by the roll-up vector $\vec{w}$ and an applied magnetic field. Hence it follows that some nanotubes are metallic with high electrical conductivity, while others are semiconducting with relatively low band gaps.

## *Band Structure of Graphene*

We describe here the band structure of carbon nanotubes by the technique of projecting the band dispersion of a 2D graphite layer into the 1D longitudinal dimension of the nanotube. The 2D band dispersion of graphene can be found in [14]. It consists of an upper and a lower branch that only touch at the corners of the hexagonal Brillouin zone. Thus, when the system is at half-filling, the metallic properties derive from a pair of inequivalent Fermi points, around which there is conical dispersion for the modes of the graphene sheet.

The 2D layer in graphite, known as *graphene* was largely studied in recent years [15] also because of the isolation of single layer graphene by Novoselov et al. [16]. One of the most interesting aspects of the graphene problem is that its low energy excitations are massless, chiral, Dirac fermions. In neutral graphene the chemical potential crosses exactly the Dirac point. This particular dispersion, that is only valid at low energies, mimics the physics of quantum electrodynamics (QED) for massless fermions except by the fact that in graphene the Dirac fermions move with a speed $v_F$ which is 300 times smaller than the speed of light, $c$. Hence, many of the unusual properties of QED can show up in graphene but at much smaller speeds [17–19]. Dirac fermions behave in very unusual ways when compared to ordinary electrons if subjected to magnetic fields, leading to new physical phenomena [20, 21] such as the anomalous integer quantum Hall effect (IQHE) measured experimentally [22, 23].

Graphene has a honeycomb structure as shown in Fig. 3. The structure is not a Bravais lattice but it can be seen as a triangular lattice with a basis of two atoms per unit cell. Of particular importance for the physics of graphene are the two points

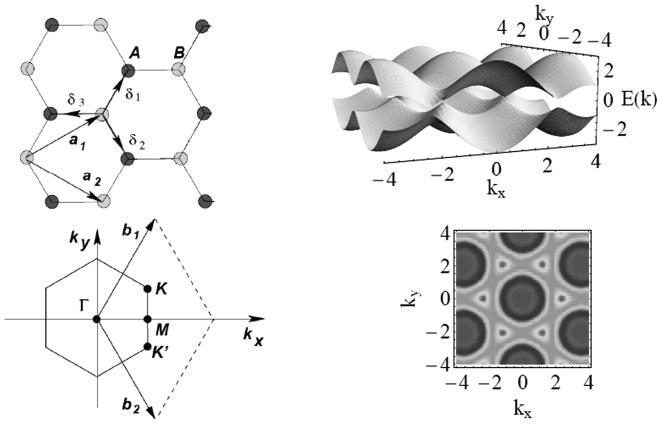


**Fig. 3** (*Top.Left*) Lattice structure of graphene, made out of two interpenetrating triangular lattices ($\mathbf{a}_1$ and $\mathbf{a}_2$ are the lattice unit vectors, and $\boldsymbol{\delta}_i, i = 1, 2, 3$ are the nearest neighbor vectors) (*Bottom.Left*) corresponding Brillouin zone. The Dirac cones sit at the K and K′ points. (*Top.Right*) Energy bands for finite v $t$ =2.7 eV and $t' = 0$, the cusps appear at the six corners of the first Brillouin zone as enphasized in panel (*Bottom.Right*) where the density plot of the energy levels in a graphite sheet is reported

$K$ and $K'$ at the corners of the graphene's Brillouin zone (BZ). These are named Dirac points. Their positions in momentum space are given by:

$$K = \left(\frac{2\pi}{3a}, \frac{2\pi}{3\sqrt{3}a}\right), \quad K' = \left(\frac{2\pi}{3a}, -\frac{2\pi}{3\sqrt{3}a}\right). \tag{1}$$

The three nearest neighbors vectors are given by, $\delta_1 = \frac{a}{2}(1, \sqrt{3})$, $\delta_2 = \frac{a}{2}(1, -\sqrt{3})$ and $\delta_3 = -a(1, 0)$, while the six second-nearest neighbors are located at: $\delta_1^{'} = \pm a_1, \delta_2^{'} = \pm a_2, \delta_3^{'} = \pm(a_2 - a_1)$.

**The Tight-Binding Approach**

The tight-binding Hamiltonian for electrons in graphene considering that electrons can hop both to nearest and next nearest neighbor atoms has the form,

$$H = -t \sum_{\langle i,j\rangle,\sigma} \left(a^{\dagger}_{\sigma,i} b_{\sigma,j} + \text{h.}c.\right) - t' \sum_{\langle\langle i,j\rangle\rangle,\sigma} \left(a^{\dagger}_{\sigma,i} a_{\sigma,j} + b^{\dagger}_{\sigma,i} b_{\sigma,j} + \text{h.}c.\right), \tag{2}$$

where $a_{i,\sigma}$ ($a^{\dagger}_{i,\sigma}$) annihilates (creates) an electron with spin $\sigma$ ($\sigma = \uparrow, \downarrow$) on site $R_i$ on sub-lattice A (an equivalent definition is used for sub-lattice B, see Fig. 2), $t$ ($\approx$ 2.8 eV) is the nearest neighbor hopping energy (hopping between different sub-lattices). Next we neglect $t'$ ($\approx$ 0.1 eV) i.e. the next nearest neighbor hopping energy (hopping in the same sub-lattice) [24]. The energy bands derived from this Hamiltonian have the form [25]:

$$E(k) = \pm t \sqrt{1 + 4\cos^2\left(\frac{\sqrt{3}}{2} k_y a_0\right) + 4\cos\left(\frac{\sqrt{3}}{2} k_y a_0\right)\cos\left(\frac{3}{2} k_x a_0\right)} \tag{3}$$

where the plus sign applies to the upper ($\pi$) and the minus sign the lower ($\pi^*$) band. It is clear from Eq. 3 that the spectrum is symmetric around zero energy. In Fig. 3. *Top.Right* we show the full band structure of graphene.

The band structure close to one of the Dirac points shows clearly a conical dispersion

$$E_{\pm}(\mathbf{q}) \approx \pm v_F |\mathbf{q}| \tag{4}$$

where $q = k - K$ is the momentum measured relatively to the Dirac points and $v_F$ represents the Fermi velocity, given by $v_F = 3ta/2$, with a value $v_F$; $1\times10^6$ m/s [25].

The most striking difference between this result and the usual case, $\varepsilon(q) = q^2/(2m)$ where $m$ is the electron mass, is that the Fermi velocity in Eq. 4 does not depend on the energy or momentum: in the usual case we have $v = k/m = \sqrt{2E/m}$ and hence the velocity changes substantially with energy.

Since the basis of the honeycomb lattice contains two atoms, there are two sub-lattices and two degenerate Bloch states at each Fermi point. If we choose the Bloch

functions separately on each sublattice such that they vanish on the other, then we can expand the electron operator in terms of the Bloch waves

$$\Psi_\sigma(x,y) : \sum_{p\alpha} \exp(-i\alpha K \cdot r) F_{p\alpha\sigma}(x,y) \tag{5}$$

where $\alpha = \pm$ labels the Fermi point, $r = (x,y)$ lives on the sublattice $p = \pm$ under consideration and $F_{p\alpha\sigma}(x,y)$ denote slowly varying operators. Thus, we can conclude that the low-energy excitations of the honeycomb lattice at half-filling are described by an effective theory of two 2D Dirac spinors [14].

## *Band Structure of Carbon Nanotubes*

Starting from the graphene band structure Eq. 3, after introducing periodic boundary conditions due to the cylindrical geometry of the tube (i.e. the wrapping vector $\overleftarrow{w}$), we can obtain the energy bands of a carbon nanotube.

### From Graphene to Carbon Nanotubes

In this section we start from Eq. 3 and discuss first the general case of Chiral CNs then the highly symmetric nanotubes, namely (1) the armchair $(n,n)$ and (2) the zig-zag $(n,0)$.

For the case of a chiral nanotube we can write the general condition

$$\vec{w} \cdot \vec{k} = 2\pi m; \quad m \in Z.$$

It follows that we can define a quantization rule,

$$\frac{\sqrt{3}a}{2}(m_w + n_w)k_x + \frac{a}{2}(m_w - n_w)k_y = 2\pi m,$$

then

$$k_x = \frac{4\pi m}{\sqrt{3}a(m_w + n_w)} + \frac{(n_w - m_w)}{\sqrt{3}(m_w + n_w)}k_y = \frac{4\pi m}{\sqrt{3}an_+} + \frac{n_-}{\sqrt{3}n_+}k_y.$$

Substitution of the discrete allowed values for $k_x$ into Eq. 3 yields the energy dispersion relations for the generic chiral tube,

$$E_m(k) = \pm t\sqrt{1 + 4\cos\left(\frac{2m\pi}{n_+} + \frac{n_-}{2n_+}k_y\right)\cos\left(\frac{\sqrt{3}k_y}{2}a_0\right) + 4\cos^2\left(\frac{\sqrt{3}k_y}{2}a_0\right)}. \tag{6}$$

In the case (1) $|2\pi R| = n|(a_1 + a_2)| = n\sqrt{3}a$. Thus due to the periodic boundary condition along the $x$ direction, the wavevector component $k_x$ is quantized,

$$k_x = m\frac{2\pi}{n\sqrt{3}a};\ \ m \in Z$$

Substitution of the discrete allowed values for $k_x$ into Eq. 3 yields the energy dispersion relations for the armchair tube

$$E_m(k) = \pm t\sqrt{1 \pm 4\cos\left(\frac{m\pi}{n}\right)\cos\left(\frac{\sqrt{3}\,k}{2}a_0\right) + 4\cos^2\left(\frac{\sqrt{3}\,k}{2}a_0\right)} \tag{7}$$

where $-\pi < ka < \pi$.

The case (2), i.e. a zigzag nanotube, is characterized by a wrapping vector in the form $(n, 0)$ or $(n, -n)$, the latter case gives a simple quantization rule in the form

$$k_y = m\frac{2\pi}{na};\ \ m \in Z$$

so that

$$E_m(k) = \pm t\sqrt{1 + 4\cos^2\left(m\frac{2\pi}{n}\right) \pm 4\cos\left(\frac{2\pi}{n}\right)\cos\left(\frac{3}{2}k_x a_0\right)}, \tag{8}$$

where $-\pi/3 < k_x a_0 < \pi/3$.

Thus we obtain that just $1/3$ of the possible nanotubes are metallic when the condition $m_w - n_w = 3q$, with $q$ integer, is fulfilled. At half-filling, metallic nanotubes have two Fermi points (see Fig. 3 *Left*) corresponding to large momenta

$$\pm K_s = \pm(2\pi)/(3a_0)$$

Here we choose a nanotube oriented as in Fig. 4. *left*, thus the low-energy expansion Eq. 5 transforms correspondingly and the electron operator reads [26]

$$\Psi_\sigma(\varphi, y) = \sum_{p\alpha} (2\pi R)^{-1/2} \exp(-i\alpha K \cdot r)\,\psi_{p\alpha\sigma}(y) \tag{9}$$

which introduces 1D fermion operators $\psi_{p\alpha\sigma}(y)$ depending only on the longitudinal coordinate $y$. The fact of having four low-energy linear branches at the Fermi level introduces a number of different scattering channels, depending on the location of the electron modes near the Fermi points.

In general, we can define an approximate one-dimensional bandstructure for momenta near $\pm K_s$

$$\varepsilon_0(m, \overleftarrow{w}, k) \approx \pm\frac{v_F\hbar}{R}\sqrt{\left(\frac{m_w - n_w + 3m}{3}\right)^2 + R^2(k \pm K_s)^2} \tag{10}$$

where $R$ is the tube radius.

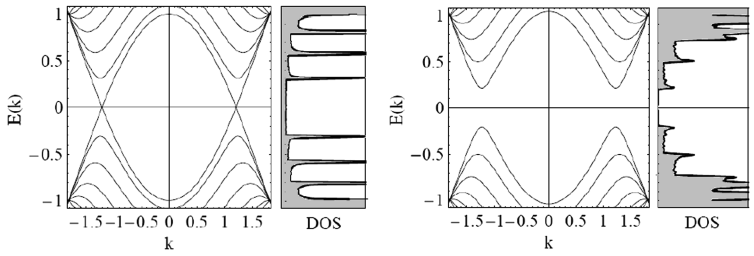


**Fig. 4** Band structure and density of states for a (10, 10) armchair nanotube within the zone-folding model. The 1D energy dispersion relations are presented in the $(-1; 1)$ energy interval in units $t$ : 2.9 eV. The Fermi level is located at zero energy. Band structure and density of states for a (20, 0) zigzag nanotube within the zone-folding model. The Fermi level is located at zero energy

For a metallic CN (e.g. the armchair one with $m_w = n_w$) we obtain that the energy vanishes for two different values of the longitudinal momentum $\varepsilon_0(\pm K_s) = 0$. As we discussed for graphene, the dispersion law $\varepsilon_0(m, k)$ in the case of undoped metallic nanotubes is quite linear near the crossing values $\pm K_s$. The linear dispersion relation holds for energy scales $E < D$, with the bandwidth cutoff scale

$$D : v_F \hbar / R \approx 0.7\, eV/R(\mathrm{nm}^{-1}),$$

which is a relevant quantity also to define a low-energy regime ($k_B T < D$). The latter regime is often met even at room temperature for usually small radius CNs.

### Dirac Fermions Approach

Starting from Eq. 10 we can develop a Dirac-like theory for CNs obtained by taking a continuum limit in which the momenta are much smaller than the inverse of the $C - C$ distance $a_0$ [27] (the continuum limit also requires $\ell_\omega^2 >> aR$ so that lattice effects can be disregarded). Thus we write the Hamiltonian, near a Fermi point, as

$$H_D = v_F \left[ \hat{\alpha}(\hat{\pi}_\varphi) + \hat{\beta}\, \hat{\pi}_y \right], \tag{11}$$

where $\hat{\pi}_\varphi = \frac{L_y}{R} = -i \frac{\hbar}{R} \frac{\partial}{\partial \varphi}$ corresponds to the momentum along the circumference of the nanotube while $\hat{\pi}_y = \hat{p}_y \pm \hbar K_s$ is the momentum along the axis. The Hamiltonian above gives a Dirac like equation which has a solution in the spinorial form $\hat{\psi}$ where

$$\hat{\alpha} = \alpha \begin{pmatrix} 0 & i \\ -i & 0 \end{pmatrix} \quad \hat{\beta} = \begin{pmatrix} 0 & 1 \\ 1 & 0 \end{pmatrix} \quad \hat{\Psi} = \begin{pmatrix} \psi_\uparrow \\ \psi_\downarrow \end{pmatrix}. \tag{12}$$

Eq. 11 can be compared with the one obtained in [28]. For the metallic CN, such as the armchair one, the problem in Eq. 11 has periodic boundary conditions

*i.e.* $\Psi(\varphi + 2\pi, y) = \Psi(\varphi)$, it follows that a factor $e^{im\varphi}$ appears in the wavefunction while for semiconducting CNs ($m_w \neq n_w$) we have to define *quasiperiodic boundary conditions i.e.* $\Psi(\varphi + 2\pi, y) = \omega\Psi(\varphi)$ [28] corresponding to a phase factor in the wavefunction $e^{i\left(m+\frac{m_w-n_w}{3}\right)\varphi}$ (next we use $m_0 = m_w - n_w$).

Thus we can trivially obtain the spinorial eigenfunctions as

$$\overset{\wedge}{\Psi}_+ = \begin{pmatrix} \cos(\gamma) \\ \sin(\gamma) \end{pmatrix} e^{i\left(m+\frac{m_w-n_w}{3}\right)\varphi} e^{iky}; \qquad \overset{\wedge}{\Psi}_- = \begin{pmatrix} -\sin(\gamma) \\ \cos(\gamma) \end{pmatrix} e^{i\left(m+\frac{m_w-n_w}{3}\right)\varphi} e^{iky}, \tag{13}$$

by choosing appropriately $\gamma$. The eigenenergies are given by Eq. 10.

Thus, in relation to the study of transport properties, often an important quantity linked to the dispersion relation is the so-called effective mass of the charge carriers. In semiconducting nanotubes, this quantity can be derived from the Eq. 10 as $m_{eff} = m + m_0$ and vanishes (massless Dirac Fermions) for the electrons belonging to the lowest subband of a metallic CN. This concept has been used [29] to estimate the charge mobility properties in semiconducting nanotubes.

### The Density of States

The density of states (DOS) $\Delta N/\Delta E$ represents the number of available states for a given energy interval $\Delta E$. This DOS is a quantity that can be measured experimentally under some approximations. The shape of the density of states is known to depend dramatically on dimensionality. In 1D, as shown below, the density of states diverges as the inverse of the square root of the energy close to band extrema. These spikes in the DOS are known as Van Hove singularities and manifest the confinement properties in directions perpendicular to the tube axis. As carbon nanotubes are one dimensional, their corresponding DOS exhibits a spiky behavior at energies close to band edges as shown in Fig. 3. The position of these Van Hove singularities can be analytically derived from the dispersion relations.

## *Magnetic Field and Landau Energy Bands of Carbon Nanotubes*

The application of a uniform external magnetic field has profound consequences on the electronic band structure of carbon nanotubes. There exist two cases of high symmetry for the direction of the magnetic field with respect to the nanotube axis (see Fig. 4).

When the magnetic field is applied parallel to the tube axis, electrons within the nanotube are influenced by the electromagnetic potential, whose dominating effect is to add a new phase factor, the Aharonov-Bohm quantum phase, to the quantum wave function with subsequent modification of the associated momentum.

When a transverse magnetic field is present, in metallic tubes were found a suppression of the Fermi velocity at half-filling and an enhancement of the density of states while in semiconducting tubes the energy gap is suppressed.

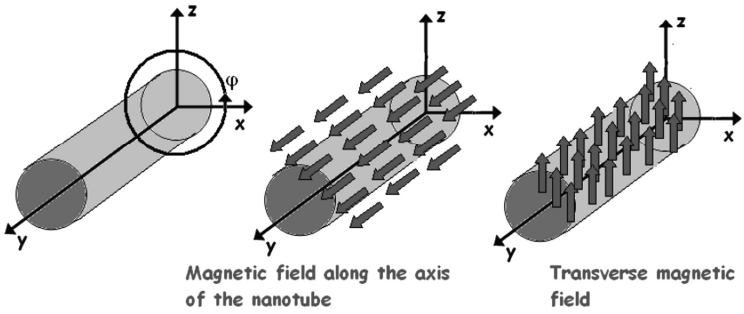


**Fig. 5** (*Left*) Schematic draw of an isolated CN with the longitudinal axis along the *y* direction. The two cases of high symmetry for the direction of the magnetic field with respect to the nanotube axis: (Middle) the magnetic field is applied parallel to the tube axis, (*Right*) the magnetic field is applied perpendicular to the tube axis

Here the electron properties of carbon nanotubes are studied using a model of a massless Dirac particle on a cylinder [30]. As it was discussed by Lee and Novikov [28] the problem possesses supersymmetry which protects low-energy states and ensures stability of the metallic behavior in arbitrarily large fields. These features qualitatively persist (although to a smaller degree) in the presence of electron interactions. Here we propose a simplified version of the theory proposed in [28] also if several works on the standard tight binding approach were presented in the last years.

### Transverse Magnetic Field

A cylindrical carbon nanotube with the axis along the *y* direction and *B* along *z*, corresponds to

$$H_D = v_F \left[ \hat{\alpha}(\hat{\pi}_y) + \hat{\beta} \left( \hat{\pi}_y - \frac{e}{c} A \right) \right], \tag{14}$$

The minimal form of the coupling to external fields follows from the gauge invariance while we choose the gauge so that the system has a symmetry along the $\hat{y}$ direction,

$$A = (0, Bx, 0) = (0, BR\cos(\varphi), 0)$$

and we introduce the cyclotron frequency $\omega_c = \dfrac{eB}{m_e c}$ and the magnetic length $\ell_\omega = \sqrt{\hbar/(m\omega_c)}$.
It is customary to discuss the results in terms of two parameters, one for the scale of the energy following from Eq. 10

$$\Delta_0 = \hbar v_F R\,, \tag{15}$$

the second one being the scale of the magnetic field

$$\nu \equiv \pi R^2 2\pi \ell_\omega^2 = \pi R^2 B \Phi_0 \quad \text{where} \quad \Phi_0 = hce. \tag{16}$$

Here we can calculate the effects of the magnetic field by diagonalizing Eq. 14, after introducing the trial functions

$$\bar{\psi}_{s,m,k}(\varphi, y) = N e^{i(ky+(m+m_0)\varphi)}\big(\alpha_s + \beta_s \sin(\varphi) + \gamma_s \cos(\varphi)\big). \tag{17}$$

Results are reported in Fig. 6 for different CNs and values of the magnetic field.

From the expression of $|\Psi_{m,\pm k}(\varphi, y)|^2$ we deduce a kind of 'edge localization' of the opposite current, analogous to the one obtained for the QW [32] also for CNs.

Following the calculations reported in [28] for a metallic CN we can easily calculate the linear dispersion relation changes near the band center $\varepsilon = 0$. Thus, the magnetic dependent energy can be written, near the Fermi points $k : K_s$, in terms of $\nu$ as

$$\varepsilon(|k - K_s|) = \pm\hbar|k - K_s|\,(v_F I_0(4\nu)) \ . \tag{18}$$

This describes a reduction of the Fermi velocity $\hbar^{-1} d\varepsilon/dk$ near $\varepsilon = 0$ by a factor $I_0(4\nu)$.

Hence, the magnetic dependent Fermi wavevector follows

$$k_F(\varepsilon_F, \nu, 0) \approx K_s + \left(\frac{\varepsilon_F}{\hbar v_F}\right) I_0(4\nu),$$

where the second term in the r.h.s. depends on $B$ as

$$k_F = K_s \pm k_0 + k(B) \approx K_s \pm k_0(1 + 4\nu^2 + ...) \to k(B) : 4k_0\nu^2,$$

where $k_0 = \left(\frac{\varepsilon_F}{\hbar v_F}\right)$.

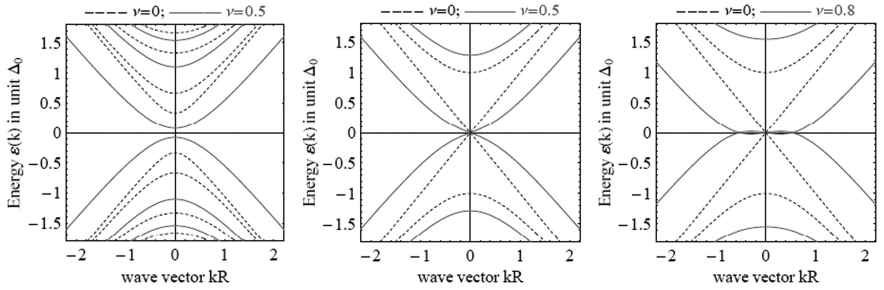


**Fig. 6** In the x-axis the wavevector in unit $(k_y - K_s)R$ $(\pi_y R/\hbar)$. (*left*) Bandstructure of a non-metallic CN with (*red lines*) and without (*black dashed lines*) the transverse magnetic field ($\nu = 0.5$). The main consequence of $B$ is the reduction of the semiconducting gap. (*Middle* and *right*) Bandstructure of a metallic CN with (*red lines*) and without (*black dashed lines*) the transverse magnetic field. The main consequence of $B$ at intermediate fields is the rescaling of the Fermi velocity, while for quite strong fields a flat zone appears near $\pi_y = 0$. We know that the magnetic parameter $\nu \approx 0.2$ for $B : 5\,T$ and $R \approx 50\,nm$ [31]

In Fig. 6 we show how the bandstructure can be modified by the presence of a transverse magnetic field. On the left we show that for a semiconducting CN the main consequence of $B$ is the reduction of the semiconducting gap. On the right we note that for metallic CNs that the gap vanishes and we get massless subbands crossing each other at zero energy. The flat region near $K_s$ correspond to the insurgence of Localized Landau levels.

The closure of the gap at a magnetic field $B < 5$ T is consistent with the results for semiconducting carbon nanotubes in [33]. From there we can infer that the magnetic field needed to close the gap of a nanotube with radius $R = 10$ nm must be of the order of 10 T. This field strength would be reduced by a factor of 4 after doubling the nanotube radius, keeping the same ratio of $R/\ell_\omega$.

The evolution of the band structure of the thick nanotubes considered here is quite different from that of carbon nanotubes with typical radius ($\approx 1$ nm) in strong magnetic fields. The latter have been investigated in [34], where typical oscillations have been reported in the low-energy levels of carbon nanotubes with $R \approx 1$ nm as the magnetic field is increased to ratios of $R/\ell_\omega = 3$. The reason why the low-energy levels do not stabilize at increasing magnetic field can be traced back to the fact that, for such thin carbon nanotubes, there is no regime where the continuum limit with $aR/\ell_\omega^2 = 1$ can be realized.

**Edge States, Landau Levels and Hall Effect**

In the section above we discussed the effects of an external magnetic field on the bandstructure of a CN. Here, following Refs. [35, 36] we discuss how, for thick carbon nanotubes in a transverse magnetic field, the transport properties can be governed by the states localized at the flanks of the nanotube, which carry quantized currents in the longitudinal direction.

The effects of a transverse magnetic field on the transport properties of the carbon nanotubes were investigated making use of the description of the electronic states in terms of Dirac fermion fields [35, 36] i.e. the discussed continuum limit. It follows that the results reported in Fig. 6.*right* are valid for thick CNs while in the cases of thin CNs where the low-energy levels do not get stabilized at increasing magnetic field, by the time that we have $R \geq \ell_\omega$, the magnetic length cannot be much larger than the $C - C$ distance, so that a quantum Hall regime cannot exist in thin carbon nanotubes. This can be also appreciated in the results of cuni [37], where the density of states of several carbon nanotubes is represented at very large magnetic fields, with a marked difference between the cases of thin and thick nanotubes. It has been shown for instance that the density of states for nanotube radius $R \approx 14$ nm already resembles that of the parent graphene system, with clear signatures of Landau subbands in the low-energy part of the spectrum.

Thus we conclude that for nanotubes with a radius $R \approx 20$ nm, in a magnetic field of $\approx 20$ T, the band structure shows a clear pattern of Landau levels. This opens the possibility of observing the quantization of the Hall conductivity in multi-walled nanotubes, $\sigma_{xy}$.

In the case of graphene, it has been shown that $\sigma_{xy}$ has plateaus at odd multiples of $2e^2/h$, as a consequence of the peculiar Dirac spectrum [20, 21]. In Refs. [35, 36]

was obtained that the different topology of the carbon nanotubes leads instead to a quantization in even multiples of the quantity $2e^2/h$, with steps in $\sigma_{xy}$ which are doubled with respect to those in graphene.

Regarding the spatial distribution, there is also a clear correspondence between the localization of the states in the angular variable $\varphi$ and the value of the current. This can be appreciated from the analysis of the eigenstates of the Hamiltonian (see Eq. 17, Fig. 6 of [35], where the angular distribution of states from the lowest Landau subband for $B = 20$ T or the schematic plot in Fig. 7).

Thus the role of the magnetic field is to separate left-moving and right-moving currents at opposite sides of the tube. The localization of the current in the states of the dispersive branches opens the possibility to observe the quantization of the Hall conductivity in thick carbon nanotubes.

Therefore the Hall conductivity, defined by $\sigma_{xy} = I/V_H$, must have a first plateau as a function of the filling level, with a quantized value given by the spin degeneracy and the doubling of the subbands

$$\sigma_{xy} = 4\frac{e^2}{h} \tag{19}$$

As the filling level is increased, the situation changes when the Fermi level starts crossing the bumps with parabolic dispersion

The contribution of each inner dispersive branch to the Hall conductivity turns out to be then smaller than the quantized value from the outermost edge states. Consequently, an approximate quantization of $\sigma_{xy}$ is observed above the first plateau, as shown in Fig. 6.*right*, with steps according to the degeneracy of the subbands:

$$\sigma_{xy} \approx (2 + 4n)2\frac{e^2}{h}. \tag{20}$$

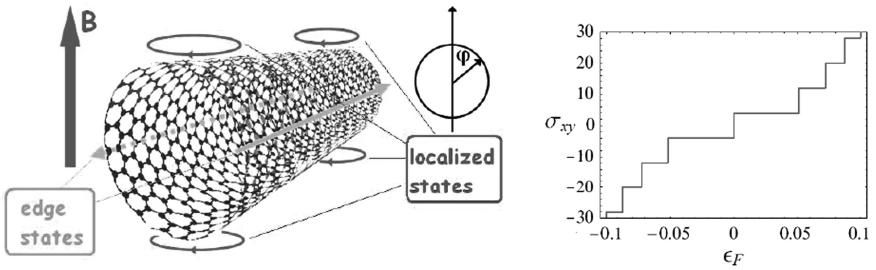


**Fig. 7** Each eigenfunction is in general localized around a certain value of the angular variable $\varphi$. We observe, for instance, that the states at $k = 0$ have wave functions localized at $\varphi = 0$ or $\varphi = \pi$, with the contribution to the current from the left component compensating exactly that from the right component. For positive (negative) longitudinal momentum, the states in the flat zero-energy level are localized at angles between 0 and $\pi/2$ ($3\pi/2$), or between $\pi$ and $\pi/2$ ($3\pi/2$), depending on the subband chosen. For the states in the dispersive branches, the eigenfunctions are centered around $\pi/2$ (for a *right* branch) or $3\pi/2$ (for a left branch). (*Right*) Plot of the Hall conductivity (in units of $e^2/h$) as a function of the position of the Fermi level $\varepsilon_F$ in the band structure for a sharp voltage drop in the bulk of the nanotube (adapted from [35])

### Magnetic Field along the Axis of the SWCNT

As we discussed above a magnetic field along the axis of the SWCNT also modifies the band structure. One way to see this is to add an Aharonov-Bohm flux term to the quantization condition

The cylindrical carbon nanotube with the axis along the $y$ direction and $B$ along $y$, corresponds to

$$H_D = v_F \left[ \hat{\alpha}(\hat{\pi}_\varphi - \frac{\hbar}{R}\frac{\Phi(B)}{\Phi_0}) + \hat{\beta}\left(\hat{\pi}_y - \frac{e}{c}A\right)\right], \tag{21}$$

As we discussed above the boundary conditions in the $\varphi$ direction are periodic for the metallic case and quasiperiodic for the dielectric case. In the presence of a parallel magnetic field the problem remains separable and thus the wave function can be factorized in just the same way as in the case of vanishing magnetic field. One again finds 1D subbands with the spectrum of Eq. 10, with an additive mass term,

$$\varepsilon_0(m,w,k) \approx \pm\frac{v_F\hbar}{R}\sqrt{\left(\frac{m_w - n_w + 3m}{3} + \frac{\Phi(B)}{\Phi_0}\right)^2 + R^2(k \pm K_s)^2} \tag{22}$$

Thus in the presence of a parallel field the gapless $m = 0$ branch of the metallic nanotube spectrum acquires a gap [40, 41]. Interestingly, there is no threshold for this effect, since the gap forms at arbitrarily weak field. The gap size is $2\Delta = 2|\frac{\Phi(B)}{\Phi_0}|\frac{\hbar v_F}{R}$. One notes that the field-induced gap appears not at the Fermi level but at the center of the electron band. Thus it affects the metallic NT properties only for electron density sufficiently close to half-filling.

The magnetic field basically shifts the quantization lines perpendicular to their direction. Because of the small diameter of the nanotubes the period to shift one quantization line to the next by the field is several thousands Tesla. However, effects due to the modification (small shifts) of the band structure with common laboratory accessible fields as $B < 10\,\mathrm{T}$ can easily be observed in low temperature experiments.

As we show in Fig. 8 a metallic armchair SWCNT can thus be made semiconducting by applying a magnetic field while for semiconducting SWCNT, the two lowest subbands are shifted in opposite directions by the field. Such a field, by inducing backscattering between right and left electron modes, opens a minigap at the band center. This gap, linear in the field (see Fig. 8.*right*), is given by the magnetic flux scaled by the flux quantum, $(\pi R^2 B/\Phi_0)$, times the semiconducting gap size. Effects of parallel field on multi-walled NT have been reported in [42]. Electronic properties are also sensitive to mechanical distortion, such as twisting, bending, or squashing, [43–47] as well as to external electric fields [48, 49].

### Aharonov-Bohm Effect

In addition to the periodic band-gap oscillations, discussed above, the Aharonov-Bohm effect more generally affects the whole subband structure, as evidenced by

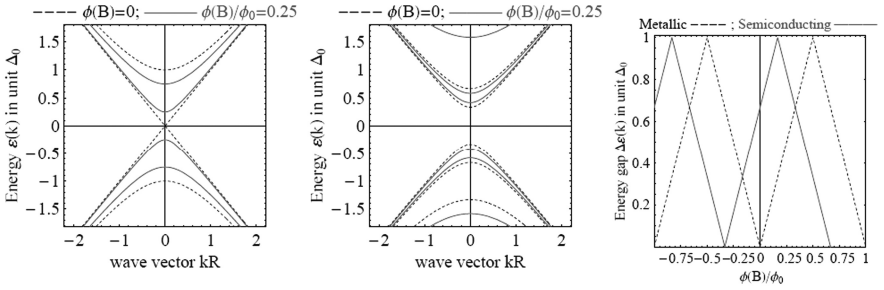


**Fig. 8** In the x-axis the wavevector in unit $(k_y - K_s)R$ $(\pi_y R/\hbar)$. (*left*) Bandstructure of a metallic CN with (*red lines*) and without (*black dashed lines*) the magnetic field (in unit $\phi/\phi_0$). This is a metallic tube at zero magnetic flux but a gap opens up once a finite flux is applied and increases with the flux. (Middle) Bandstructure of a semiconducting CN with (*red lines*) and without (*black dashed lines*) the parallel magnetic field. (*Right*) The energy gap modified by applying a finite magnetic flux threading the tube: for a metallic CN the band gap opens and increases linearly with $B$, to reach a maximum value at half the quantum flux $\phi/\phi_0 = 1/2$. Further, the band gap, $\Delta E$ is linearly reduced until it finally closes back when the field reaches one quantum flux. The behaviour of a semiconducting CN is analogous and is represented by a shifted curve in the plain $\phi - \Delta E$ [33, 38, 39]

Van Hove singularity splitting and shifts [50–52]. In the Aharonov-Bohm effect [53, 54] a beam of quantum particles, such as electrons, is split into two partial beams that pass on either side of a region containing a magnetic field, and these partial beams are then recombined to form an interference pattern. The interference pattern can be altered by changing the magnetic field – even though the electrons do not come into contact with the magnetic field see Fig. 9.

Thus the large diameter of MWNTs enables one to investigate quantum-interference phenomena in a magnetic field and especially the AB effect that not only reveals that electrons are waves, but also demonstrates that the vector potential not the magnetic field plays a basic role. For the study of this phenomenon, a magnetic field of several Tesla was applied along the nanotube axis. The electrical resistance measurements showed pronounced oscillations with a period of $h/2e$, as in Fig. [9]. The oscillations are associated with the 'weak localization', a quantum-mechanical manifestation of coherent backscattering of electrons, which arises from interference contributions adding up constructively in zero field. Backscattering is thereby enhanced, leading to a resistance larger than the classical Drude resistance. This observation has given compelling evidence that the phase coherence length, can exceed the circumference of the tube.

In Ref. [55] magnetoresistance measurements on individual multi-walled nanotubes, which display pronounced resistance oscillations as a function of magnetic flux were reported (see Fig. 9.*right*). It was found that the oscillations were in good agreement with theoretical predictions for the Aharonov-Bohm effect in a hollow conductor with a diameter equal to that of the outermost shell of the nanotubes.

More recently experiments on magnetoconductance in ballistic multiwalled carbon nanotubes threaded by magnetic fields as large as 55 T. In the high temperature

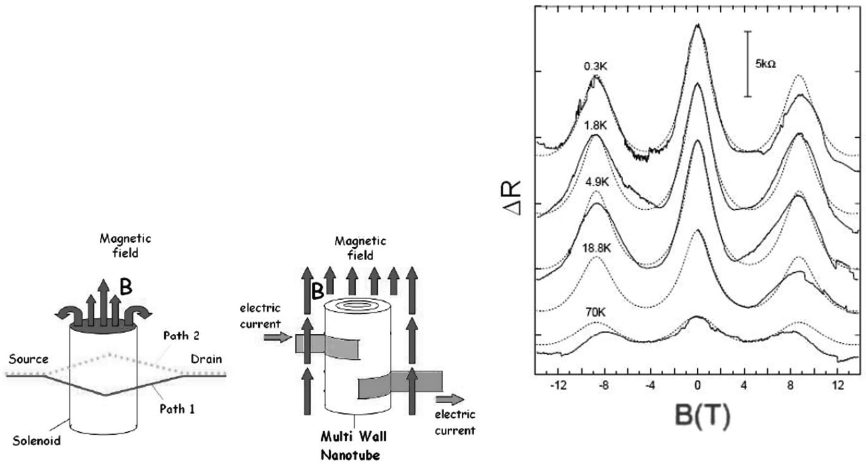


**Fig. 9** In the standard Aharonov-Bohm effect the magnetic flux through the solenoid changes the relative phase of the electron waves in paths 1 and 2, leading to the formation of an interference pattern on the screen. When the flux is changed, the interference pattern shifts on the screen. (middle) Imagine a carbon nanotube placed in a magnetic field with its axis parallel to the field. Since nanotubes are cylindrical conductors, the electrons can propagate in either the clockwise or the anticlockwise direction. These two 'paths' interfere, resulting in a periodic modulation of the electrical resistance as the magnetic flux through the tube is changed. In a carbon nanotube, the two paths are clockwise and anticlockwise around the nanotube, and the shift in the interference pattern manifests itself as a change in the electrical resistance along the nanotube as a function of magnetic field (*bottom*). The magnetic field at the peaks can be related to the quantum of magnetic flux and the cross-section of the nanotube. This effect is relatively robust and can be observed even if the electron transport in the nanotube is diffusive. In the right panel the measured magnetoresistance $R(B)$ at different temperatures $T$ for a MWNT in a parallel magnetic field $B$, from [55]

regime (100°K), giant modulations of the conductance, mediated by the Fermi level location, are unveiled. The experimental data, consistent with the field-dependent density of states of the external shell, gave a first unambiguous experimental evidence of Aharonov-Bohm effect in clean multiwalled carbon nanotubes [56].

For what concerns SWNTs, as we showed above, theoretically the AB effect manifests itself in a SWNT by periodically modifying its band structure with a period of 1 $\Phi_0$ in a magnetic flux (see Fig. 8.*right*) and about 1,000 T in field. However in a recent letter [57] it was shown that relatively low magnetic fields applied parallel to the axis of a chiral SWNT are found to cause large modulations to the p channel or valence band conductance of the nanotube in the Fabry-Perot interference regime. Beating in the Aharonov-Bohm type of interference between two field-induced nondegenerate subbands of spiraling electrons is responsible for the observed modulation with a pseudoperiod much smaller than that needed to reach the flux quantum $\Phi_0$ through the nanotube cross section. Thus was shown that single-walled nanotubes represent the smallest cylinders exhibiting the Aharonov-Bohm effect with rich interference and beating phenomena arising from well defined molecular orbitals reflective of the nanotube chirality.

## *Spin Orbit Coupling in Carbon Nanotubes*

The Spin Orbit interaction is a quantum relativistic effect due to the attractive potential of neighboring carbon atoms. It is given by

$$H_{SO} = \frac{\hbar}{4m^2c^2}\,(\nabla V \times p)\cdot\sigma,$$

where $V(r)$ is the atomic potential, $m$ the free electron mass, $p$ the electron momentum and $\sigma$ the Pauli′s spin matrix.

Recently it has been proposed that a small gap can open on the two Dirac points of graphene due to spin-orbital coupling (SOC) [58], which at the same time makes the system a spin-Hall insulator [59] with quantized spin Hall conductance. However it was shown [60] that while the spin-orbit interaction in graphene is of the order of 4 meV, it opens up a gap of the order of $10^{-3}$meV at the Dirac points, thus the predicted quantum spin Hall effect in graphene can only occur at unrealistically low temperature. The SOC effects was recently largely investigated [61, 62] also in CNs. In some papers was shown that local curvature of the graphene sheet induces an extra spin-orbit coupling term, thus the effect of SOC on derived materials of graphene like CNs can give a significant contribution.

We report here some results presented in a recent paper [63] and in agreement with previous calculations [62]. As we discussed above a continuum model for the effective spin orbit interaction in graphene can be derived from a tight-binding model which includes the $\pi$ and $\sigma$ bands and the combined effects of the intra-atomic spin orbit coupling ($\Delta$) and curvature was analyzed. Thus was shown that local curvature of the graphene sheet induces an extra spin-orbit coupling term $\Delta_{curv} \propto \Delta$, similar to the Rashba interaction due to the electric field.

Although the spin-orbit coupling for flat graphene is rather weak, some significant effects can be found in CNs, especially when their radius is quite small in fact curvature effects on the scale of the distance between neighboring atoms could increase the strength of the spin-orbit coupling at least one order of magnitude with respect that obtained for a flat surface. In a curved graphene sheet, a hopping between the orbitals in the $\pi$ and $\sigma$ bands is induced [62]. This hopping terms break the isotropy of the lattice and lead to an effective anisotropic coupling between the $\pi$ and $\sigma$ bands in momentum space.

Here we start from Eq. 11. We use cylindrical coordinates, $y, \phi$, and define the spin orientations $|\uparrow\rangle, |\downarrow\rangle$ as parallel and antiparallel to the $y$ axis. Thus we introduce in the boundary $\nu \equiv (m_w - n_w + 3m)/3$. After integrating over the circumference of the CN $\int d\phi$, the Hamiltonian of a CN including SOC reads

$$H_{S-OR}\begin{pmatrix}|A\tau\rangle\\ |B\tau\rangle\end{pmatrix} = \begin{pmatrix} 0 & \hbar(k - i\nu/R)\hat{1} + \tau i\Delta_R\pi\hat{\sigma}_z \\ \hbar(k + i\nu/R)\hat{1} - \tau i\Delta_R\pi\hat{\sigma}_z & 0 \end{pmatrix} \begin{pmatrix}|A\tau\rangle\\ |B\tau\rangle\end{pmatrix} \tag{23}$$

where the $\tau = \pm 1$ corresponds to the $K(K')$ Dirac point, $|A\tau\rangle$ are envelope functions associated to the $K$ and $K'$ points of the Brillouin zone and corresponding to states located at the $A$ and $B$ sublattices, respectively. Notice that $H$ has to be taken as a $4 \times 4$ Matrix, while $\hat{1}$ is the identity in the space of the spin. The basis states $|A\tau\rangle$ and $|B\tau\rangle$ are also spinors in spin subspace where the matrix $\hat{s}_z$ acts on with the spin orientations $|\uparrow\rangle, |\downarrow\rangle$ defined along the nanotube axis. This is different from the approach reported in [62] where the spins are defined perpendicular to the nanotube surface. However the spin-orbit term $i\Delta_R \pi \hat{s}_z$ is equivalent to the term proportional to $\hat{\sigma}_y$ obtained by Ando [62] while the the results obtained by applying Eq. 23 are in agreement with the ones reported in [61].

It follows that an energy gap $\pi\,\Delta_{\mathrm{R}}$ appears also for metallic CNs at low energies [62, 64]. This gap can be seen as a consequence of the Berry phase gained by the electron after completing a closed trajectory around the circumference of the CN under the effect of SOC ($\Delta_{\mathrm{R}}$) [62]. As a further effect $\Delta_{\mathrm{R}}$ can also give rise to a small spin splitting [62, 64]

$$\varepsilon_q = \pm \frac{\hbar v_F}{R} \sqrt{z^2 + (q^2R^2 + \nu^2) + 2\nu z \hbar \hat{s}_z}, \tag{24}$$

where $q = k \pm K_s$ and $z = \pi \frac{R\Delta_R}{\hbar v_F}$. Now we want focus on the role of the curvature in small radius CNs. In fact it results that in absence of an external electric (Rashba) field ($E$ =0). For a single wall nanotube of radius $R$ we get $R\Delta_R$ : 6.5 meV Å (see [63]) to be compared to $\hbar v_F$ : 5 eV Å.

This effect can modify in a significant way the Fermi velocity for small radius CNs. Here we limit ourselves to the case of metallic CNs and to the lowest band so that, from Eq. 24 we obtain

$$\tilde{v}_F(\varepsilon_F) = \frac{\partial \varepsilon}{\hbar \partial k} = v_F \sqrt{1 - \left(\frac{\pi\,\Delta_R}{\varepsilon_F}\right)^2}, \tag{25}$$

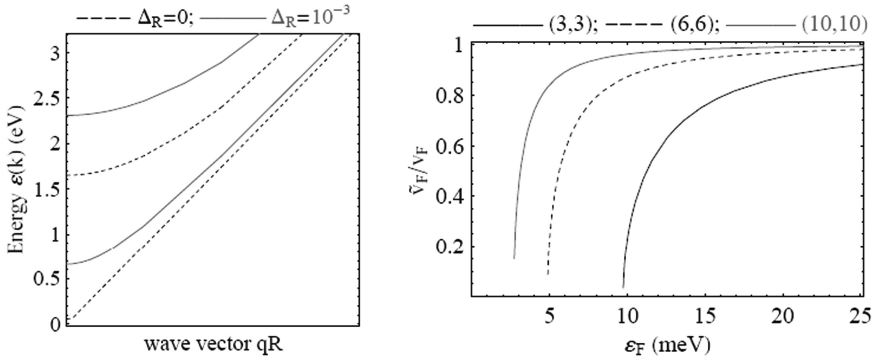


**Fig. 10** (*Left*) Bandstructure of a metallic CN modified by the SOC. (*Right*) The renormalized Fermi velocity for three different metallic CNs as $(10, 10)$ ($R$ : 7Å), $(6, 6)$ (($R$ : 4Å) and $(3, 3)$ ($R$ : 2Å) armchair ones

where $\varepsilon_F$ can be taken as the doping level. The renormalized Fermi velocity for three different metallic CNs as $(10, 10)$, $(6, 6)$ and $(3, 3)$ armchair ones is plotted in Fig. 9 where also the corrections to the banstructure are reported.

## Quantum Transport in Carbon Nanotubes

### *Ballistic Transport*

When the length of the conductor is smaller than the electronic mean free path, then the electronic transport is ballistic. This ballistic regime refers to the transport of electrons in a medium where the electrical resistivity due to the scattering, by the atoms, molecules or impurities in the medium itself, is negligible or absent.

#### Conductance Quantization

The ballistic one-dimensional wire is a nanometric solid-state device in which the transverse motion (along $\varphi$ for the CN in Fig. 5) is quantized into discrete modes, and the longitudinal motion ($y$ direction for the for the CN in Fig. 5) is free. In this case, electrons propagate freely down to a clean narrow pipe and electronic transport with no scattering can occur. In this case each transverse wave guide mode or conducting channel contributes $G_0 = e^2/h (\approx 12.9\,\mathrm{k}\Omega)$ to the total conductance. Calculations indicate that conducting single-shell nanotubes have two conductance channels [39, 40, 65]. This predicts that the conductance of a single-wall nanotube is independent of diameter and length, i.e. according to the Landauer formula [66],

$$G(E) = \frac{2e^2}{h} N_\perp(E). \tag{26}$$

This value accounts for the contribution of the two spin projections and the two propagating modes of the nanotubes, while $N_\perp(E)$ is the energy-dependent number of available quantum channels.

Thus in the case of perfect (reflection less) or ohmic contacts between the CNT and the metallic voltage probes the expected energy-dependent conductance is easily obtained, from band structure calculations, or from the DOS, by counting the number of channels at a given energy. As we show in Fig. 11 a metallic nanotube present two quantum channels at the Fermi energy $E = 0$, or charge-neutrality point, resulting in $G(0) = 2G_0$. At higher energies, the conductance increases as more channels become available to conduction.

Thus in the ideal case CNs conduct current ballistically and do not dissipate heat. The nanotubes are several orders of magnitude greater in size and stability than other typical room-temperature quantum conductors.

The quantization of the conductance has been observed at room temperature in fibers of multiwall nanotubes [68]. The experimental method involved measuring the conductance of nanotubes by replacing the tip of a scanning probe microscope

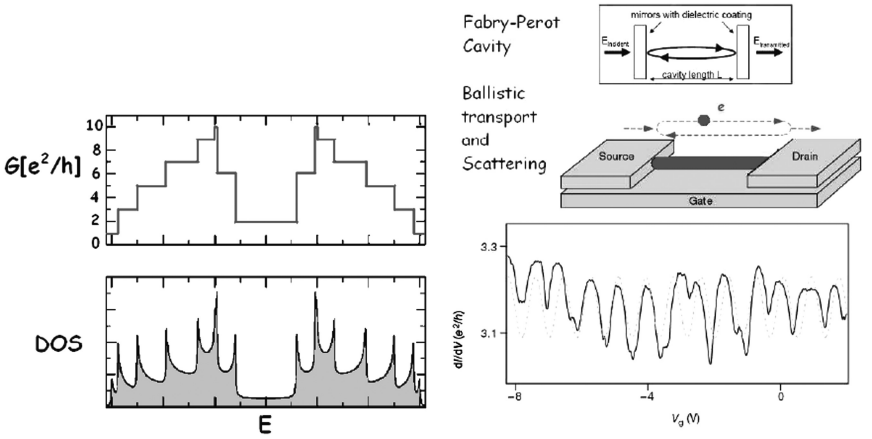


**Fig. 11** (*Right*) Density of states and ideal ballistic conductance for a metallic nanotube. (*Left*) Schematic diagram of a SWNT device illustrating the multiple electron reflection that gives rise to the observed interference pattern. Below $T = 10°\mathrm{K}$ oscillations in $\partial I/\partial V$ which are quasiperiodic in $V_g$ due to resonant tunneling. Average differential conductance around $3.2e^2/h$. Adapted from [67]

with a nanotube fiber. The conductance of arc-produced MWNTs is one unit of the conductance quantum $G_0$. Since multiwall nanotubes consist of several concentrically arranged single-wall nanotubes, one would not expect them to behave as one-dimensional conductors. If adjacent carbon layers interact as in graphite, electrons would not be confined to one layer. The results of [68] suggest, however, that the current mainly flows through the outermost layer. However the coefficent of the conductance quantum was found to have some suprising integer and noninteger values, such as $0.5G_0$. Thus in a more recent letters [69] the authors, using a scattering technique calculated the ballistic quantum conductance and found that interwall interactions not only block some of the quantum conductance channels, but also redistribute the current nonuniformly over individual tubes across the structure. these results provide a natural explanation for the unexpected integer and noninteger conductance values reported for multiwall nanotubes in [68].

Some other experiments on metallic tubes have measured only a single channel $G_0$ at low bias, instead of the two theoretically predicted channels. Several theoretical papers have proposed an interpretation in terms of the hybridization between carbon and metal orbitals at the contact [70–77]. For higher bias voltage between conducting probes, in order to explain the experimental observation of limited turn-on current with increasing bias voltage, was supposed that the modifications of bands along the tube axis produce additional backscattering analogous to a Bragg reflection [78].

In more recent experiments was shown that also single-walled carbon nanotubes are 1D conductors that exhibit ballistic conduction [67, 79–82]. In Ref. [83] was shown a nonlinear resistance vs distance behavior as the nanotube is probed along

its length. This is an indication of elastic electronic transport in one-dimensional systems. This has been related to the ballistic transport in single wall nanotube.

### Fabry-Perot Interference

In the ballistic regime the discussed wave nature of the propagating electrons yields also some interesting interference effects as the famous Fabry-Perot interference, light interference in cavity between multiply reflected light waves (see Fig. 10). In this case an analogous quantum interference can be observed between multiply reflected electron waves.

The latter interference becomes increasingly important, leading to dramatic changes in device properties when the size of a device becomes comparable to the electron coherence length [84–91], in a typical quantum ballistic regime which replaces the classical diffusive motion of electrons. The classical-to-quantum transition in device behaviour suggested the possibility for nanometer-sized electronic elements that make use of quantum coherence [84, 85, 90, 91] and among these CNs were promising candidates for realizing such device elements.

In Ref. [67] an example of a coherent molecular electronic device whose behaviour is explicitly dependent on quantum interference between propagating electron waves – a Fabry–Perot electron resonator based on individual single-walled carbon nanotubes with near-perfect ohmic contacts to electrodes. In these devices, the nanotubes act as coherent electron waveguides [68, 92, 93], with the resonant cavity formed between the two nanotube–electrode interfaces. The results were explained by using a theoretical model based on the multichannel Landauer–Buttiker formalism [94–96] to analyze the device characteristics and find that coupling between the two propagating modes of the nanotubes caused by electron scattering at the nanotube–electrode interfaces is important. in this model the nanotube is considered as a coherent waveguide with two propagating modes.

Thus in Ref. [67] a clear signature of interference effects was measured in the $\partial I/\partial V$ plots as a function of $V$ and $V_g$ measured at low temperatures. The data clearly indicated that the electrical behaviour of these nanotube devices is distinct from those reported that exhibited a Coulomb-blockade behaviour. An accurate data analysis provided experimental evidence that the electron scattering occurs mostly at the nanotube–metal interface and that electrons pass through the nanotube ballistically. A schematic diagram of a SWNT device illustrating the multiple electron reflection that gives rise to the observed interference pattern is reported in Fig. 11.

## *Coulomb-Blockade Regime*

For low contact resistances transport is mainly determined by quantum interference discussed above whereas for high contact resistances, a nanotube can behave as a quantum dot, in which Coulomb blockade determines the transport properties, Here we discuss the latter regime in detail.

### The Coulomb-Blockade Regime: General Theory

When two contacts not highly transparent are attached to a small device (next island or Quantum Dot (QD)), the measurements of the conductance and the differential conductivity reflect the strong Coulomb repulsion in the island. For temperatures that are typically below 1°K, the zero-bias conductance shows oscillations as a function of the gate voltage. This is characteristic of the so-called Coulomb blockade (CB) regime [97, 98], and the gate voltage between two peaks is related to the energy required to overcome the Coulomb repulsion when adding an electron between the barriers created by the contacts [99, 100]. Thus in these devices, because the thermal energy $k_BT$ is below the energy for adding an additional electron to the device ($\mu_N = E(N) - E(N-1)$), low bias (small $V_{sd}$) transport is characterized by a current carried by successive discrete charging and discharging of the dot with a just one electron.

This phenomenon, known as single electron tunneling (SET or quantized charge transport), was observed in many experiments in vertical QDs at very small temperature [101–103]. In this regime the ground state energy determines strongly the conductance and the period in Coulomb Oscillations (COs). COs correspond to the peaks observed in conductance as a function of gate potential ($V_g$) and are crudely described by the Coulomb Blockade mechanism [104]: the $N-th$ conductance peak occurs when [105] $\alpha e V_g(N) = \mu_N$ where $\alpha = \frac{C_g}{C_\Sigma}$ is the ratio of the gate capacitance to the total capacitance of the device (see Fig. 12).

The peaks and their shape strongly depend on the temperature as explained by the Beenakker formula for the resonant tunneling conductance [104, 106]

$$G(V_g) = G_0 \sum_{q=1}^{\infty} \frac{V_g - \mu_q}{k_B T \sinh\left(\frac{V_g - \mu_q}{k_B T}\right)} \tag{27}$$

here $\mu_1, \ldots, \mu_N$ represent the positions of the peaks.

### Microscopic Models

Here we introduce a simple microscopic model, which was developed for a metallic CN but can be easily extended to general CNs.

In a previous section we introduced the energy dispersion (Eq. 10) $\varepsilon(\vec{w}, m, k)$ by assuming an ideal CN of infinite length. When we take into account a CN between two contacts at a fixed distance ($L$) we can assume L as the CN length. It follows the quantization in the dispersion relation due to the finite longitudinal size of the tube, obtained by replacing the continuous values of $k$ with the discrete values $k_n = n\pi/L$. The longitudinal quantization introduces a parameter which also gives a thermal limit for the atomic like behavior: in fact $k$ wave vectors have to be taken as a continuum if $k_BT$ is as a critical value $\varepsilon_c = v_F(h/L)$ and as a discrete set if the temperature is below (or near) $\varepsilon_c$.

Thus we can write the single electron energies near the Fermi points as

$$\varepsilon^{\vec{w}}_{n,m,p,s} \to \varepsilon_k \approx v_F \hbar \left( |n\frac{\pi}{L} - \alpha K_s| \right) \equiv v_F \bar{k},$$

the expression in the right corresponding to the lowest subband of a metallic CNs. Thus we introduce different operators for the electrons belonging to each branch: right going operators $c^{\dagger}_{R,\bar{k},s}$ and left going ones $c^{\dagger}_{L,\bar{k},s}$ for electrons with $\bar{k} > 0$ ($\bar{k} < 0$). In terms of these operators the free and interaction Hamiltonians can be written as

$$H_0 = v_F \sum_{\bar{k},s} \bar{k} c^{\dagger}_{R,\bar{k},s} c_{R,\bar{k},s} + v_F \sum_{\bar{k},s} \bar{k} c^{\dagger}_{L,\bar{k},s} c_{L,\bar{k},s} \tag{28}$$

$$H_{int} = \frac{1}{L} \sum_{k,k',q,s,s'} \left( V^{s,s'}_{k,p}(q) c^{\dagger}_{k+q,s} c^{\dagger}_{p-q,s'} c_{p,s'} c_{k,s} \right). \tag{29}$$

Here $c_k \equiv c_{R,k}$ if $k > 0$ and $c_k \equiv c_{L,k}$ if $k < 0$, while $V^{s,s'}_{k,p}(q)$ is the Fourier transform of the electron electron interaction.

Starting from the Hamiltonian above it is possible to take into account both the correlation effects and the influence of the long range component of the e–e interaction. However a short ranged interaction model [107] can simplify the calculations of the energies of the electrons in the QD. The Hamiltonian obtained by summing

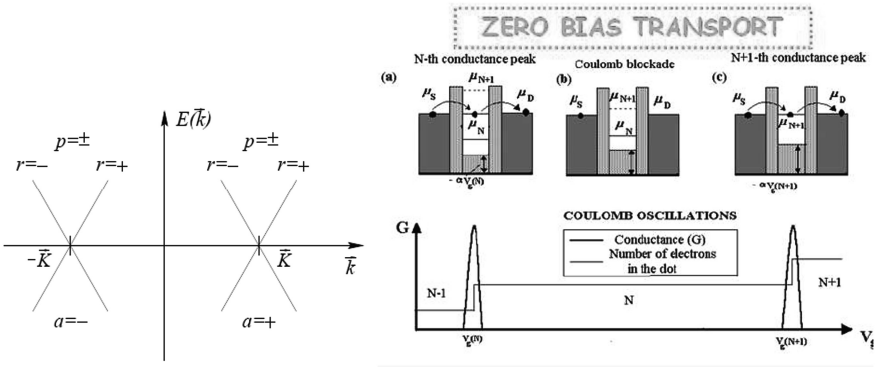


**Fig. 12** (*Left*) The Model with linearized subbands near the Fermi points for a metallic CN. (*Right*) When the contacts are not highly transparent the conductance and the differential conductivity reflect the strong Coulomb repulsion in the CNs. (*Right*) In nanometric devices, when the thermal energy $k_B T$ is below the energy for adding an additional electron to the device $\mu_N = E(N) - E(N-1)$ Thus the low bias (small $V_{sd}$) transport is characterized by a current carried by successive discrete charging and discharging of the device with just one electron. It follows that the ground state energy determines strongly the conductance and the period in Coulomb Oscillations (COs).These COs correspond to the peaks observed in conductance as a function of gate potential $V_g$. The N-th conductance peak occurs when $\alpha e V_g(N) = \mu_N$. The Addition Energy needed to place an extra electron in the device is analogous to the electron affinity for a real atom $E^A_N = \mu_{N+1} - \mu_N$

Eqs. 28 and 29 in this approach just depends on two interaction parameters [107], $J$ and $V_0$ so that

$$H = \sum_{n,\zeta,p,s} \varepsilon_{n,\zeta,p} \hat{n}_{n,\zeta,p,s} + V_0 \frac{N(N+1)}{2} - J \sum_{n,\zeta,p,s} \sum_{n',\zeta',p',s} \delta_{s,s'} \hat{n}_{n,\zeta,p,s} \hat{n}_{n,\zeta,p,s} \quad (30)$$

**Symmetries in the Bandstructure.** For a metallic CN near each Fermi point we obtain that the Hamiltonian above is represented by a typical bandstructure with linear branches depending on $\bar{k} = k + \alpha K_s$ ($\alpha = \pm 1$ labels the Fermi point). After the quantization, in the ideal case, we obtain shells with an 8-fold degeneracy (due to $\sigma$ (spin symmetry), $\alpha$ ($K, -K$ lattice symmetry), $\zeta$ ($(k-K),(K-k)$) (see Fig. 13.C.*left*).

However some asymmetries in the bandstructure were both predicted and observed. In order to take into account the strong asymmetries measured we modify the dispersion relation. A first correction has to be introduced because of the *'longitudinal incommensurability'*: in general $K$ is not a multiple of $\pi/L$ so $K = (N + \delta N)\frac{\pi}{L}$ with $\delta N < 1$ and the energy shift is $\Delta\varepsilon = v_F \frac{h\delta N}{L}$. A second correction is due to the subband mismatch ($\delta_{SM}$). The single electron energy levels are:

$$\varepsilon_{l,\sigma,p} = \hbar v_F |l\frac{\pi}{L} + pK| + \frac{(1-p)}{2}\delta_{SM} \quad (31)$$

where $p = \pm 1$.

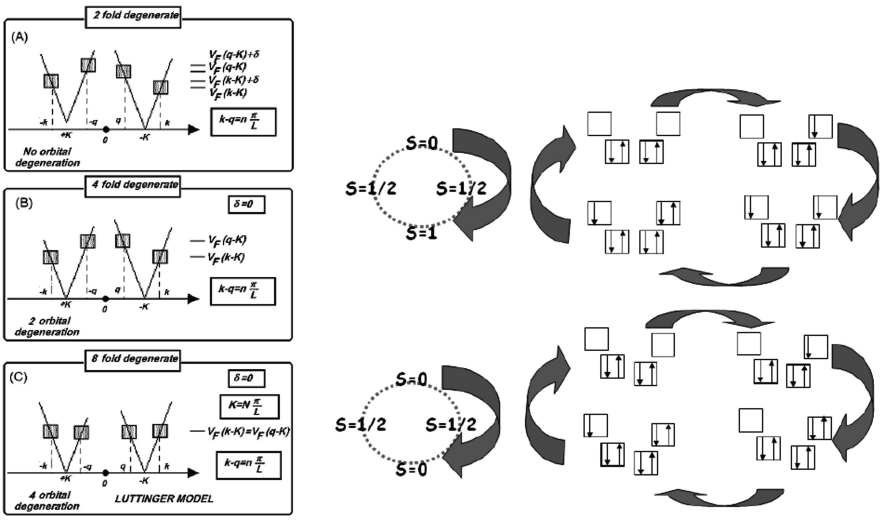


**Fig. 13** (*Left*) The dispersion relation and the quantized levels. The boxes in the figure represent energy levels and can be filled by a pair of electrons with opposite spins. (**a**) The general case without any degeneracy. (**b**) The fourfold degeneracy case. (**c**) The eightfold degeneracy case. (*Left*) A simple scheme for the aufbau which takes in account the spin in the dot. (*Top*) The degenerate case with the spin period $=, 1/2, 1, 1/2, 0$. (*Bottom*) The non degenerate case with spin period $0, 1/2$

Each choice of parameters gives a different degeneracy for the quantum levels: 8-fold degeneracy corresponds to $\delta_{SM} = 0$ and $K = n\frac{\pi}{L}$; 4-fold degeneracy is found if we put just $\delta_{SM} = 0$ and 2 fold degeneracy in the general case.

Next we just consider particles near the same Fermi point and do not take into account the labels $\alpha$. Obviously we have to consider also $\alpha - \alpha'$ interaction for particles near two different Fermi points.

## Experiments and Theoretical Results about Coulomb Blockade

Many experiments showed Coulomb Oscillations in Carbon Nanotubes e. g. in 1997 Bockrath and coworkers [97] in a rope below about 10°K observed dramatic peaks in the conductance as a function of the gate voltage that modulated the number of electrons in the rope. These typical Coulomb blockade peaks in the zero bias conductance allowed to investigate the energy levels of interacting electrons. In fact in CB a CN behaves as an artificial atom and reveals its shell structure [98]. In this sense the measurements reported in [108] (see Fig. 14.*left*) for clean 'closed' nanotube dots showed complete Coulomb blockade and enable to deduce some properties from the addition energy of SWCNT. This 'addition energy', $E_A(n)$ is the energy needed to place an extra electron (the $n$-th) in a QD, defined analogously to the electron affinity for a real atom. It was extracted from measurements as $E_A \propto \Delta V_g$. Thus was possible discuss the role which the Coulomb interaction could play in a 1D at small temperatures($T = 0.1 \div 0.3°K$).

In Fig. 14.*left*, the small bias experimental conductance $dI/dV$ as a function of gate voltage is shown. The SET prevails as revealed by the fine structure of the

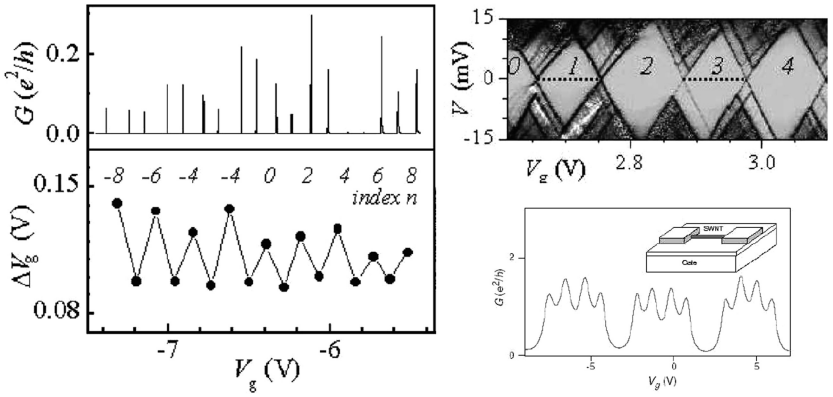


**Fig. 14** (*Left*) Conductance vs gate voltage for a nanotube quantum dot at $T = 300$ mK with evident Coulomb blockade peaks. Spacings $\Delta V_g$ of the peaks in. The index n counts the added electrons relative to an arbitrary zero. For clarity only even n's are indicated. (*Right*) A greyscale plot (darker = more positive) of $dI/dV$ vs $V_g$ and $V$ at $T = 100$ mK. The index n counts electrons added relative to the leftmost diamond. From Refs. [108, 109]

conductance spectrum. Each conductance peak represents the addition of an extra charge to the nanotube. The periodicity of the peaks is related to the size of the coherent conducting island. In the case of an irregular conductance spectrum, the nanotube is believed to be split into a series of conducting parts separated by local tunneling contacts.

The overall diagram of conductance of a QD as a function of bias and gate voltage generally appears as a diamond shaped structure referred to as the Coulomb diagram (see Fig. 14.*top.right*). For a fixed gate voltage, the current increases step wise with increasing bias voltage, producing the excited-state spectrum. Each step in the current is related to a new higher-lying energy level that enters the bias window. Within each diamond, the electron number of the nanotube is fixed and the current vanishes. The boundary of each diamond represents the transition between $N$ and $N + 1$ electrons, and the parallel lines outside the diamonds correspond to excited states. Such a plot is well understood within the constant-interaction model (Eq. 30).

Some significant deviations from this simple picture were, however observed [110]. The ground-state spin configuration in a nanotube was determined by studying the transport spectrum in a magnetic field [111]; for a metallic CN the total spin of the ground state alternates between 0 and 1/2 as successive electrons are added, demonstrating a simple shell-filling, or even-odd, effect, i.e., successive electrons occupy the levels in spin-up and spin-down pairs (see Fig. 13.*right*). The semiconducting case was analyzed in [112]. In Ref. [113] the authors used magnetic field effect to lift the orbital degeneracy thus they were able to estimate some value of the orbital magnetic moment.

The CB measurements on suspended single-wall carbon nanotubes have also shown spectacular signatures of phonon assisted tunneling, mediated by stretching modes [114].

**Effects of long range interaction.** In Ref. [115] the effects of the long range terms of the interaction in a SWNT were investigated and the results were compared with the experiments at very low temperature $T$ [108]. Thus was explained the observed damping in the addition energy for a SWNTs [108] at $T : 200\,\mathrm{mK}$ as an effect of the long range of the e–e repulsion.

In order to investigate the effects on low dimensional electron systems due to the range of electron electron repulsion, was introduced a model for the interaction which interpolates well between short and long range regimes. This model predicts oscillations in the addition energy due to the Hund′s Rule quite similar to the ones observed in QDs (usually the Interaction between the electrons with momenta near the 2 Fermi Points is very small so that we have two independent 4-fold Degenerate Hamiltonians). The oscillations periodicity is 4 for the Model (8 for a system with two Fermi points, see Fig. 13.*right*). The oscillations amplitude is due to an exchange term corresponding to the short range interaction and the effect of a long range interaction is a damping of the oscillations when the number of electrons in the System increases (compare Fig. 15.*left* with the theoretical predictions in Fig. 15.*right*).

**Asymmetries in the bandstructures** The calculations above were based on the symmetric subbands. However the real band structures of measured CN's can show

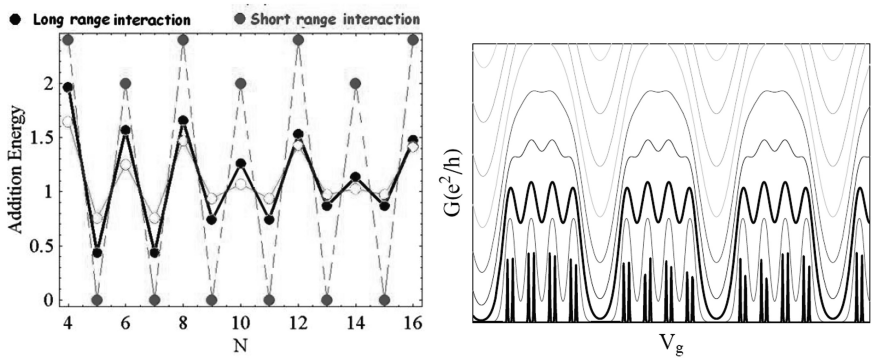


**Fig. 15** On the left the analytical Aufbau results for the addition energy versus the number of electrons of a four fold degeneracy model corresponding to different values of the range (long range *black*, short range *dashed red line*). We show how the damping in the oscillations is due to a long range interaction while it does not appear for a short range model. The predictions can be compared with the measured addition energy in the experiment of [118]. (*Right*) COs conductance vs gate voltage at different temperatures calculated following the classical CB theory. Theoretical calculations show that the fine structure peaks are appreciable just for very low temperatures (*bottom black line*)

some differences with respect to the ideal case discussed above. In fact some experiments in recent years do not find this high symmetry as result and some different hypotheses in order to explain this discrepancy were formulated.

As was discussed in [115] this symmetry has relevant effects on the *Aufbau* of the CN's shells i.e. on the spin oscillations (see Fig. 15). In the experiments reported in [109] two different shell filling models are put forward: the first one, when the subband mismatch dominates, predicts that the spin in the SWCNT oscillates between $S = 0$ and $S = 1/2$ while when the subband mismatch is negligible the spin in the SWCNT oscillates between $S = 0$, $S = 1/2$ and $S = 1$ (see Fig. 13.*right*). In Ref. [108] the authors say *'the sole orbital symmetry is a two-fold one, corresponding to a K-K′ subband degeneracy and resulting from the equivalence of the two atoms in the primitive cell of graphene structure'*.

A secondary effect of the asymmetry in the Bandstructure is related to the positions of the CB peaks in the plot $V_g - G$. Thus experimentally we can understand the symmetry properties of a CN by observing the grouping of the peaks in the conductance versus gate potential. Thus in the experiment reported in [108] no four-fold grouping was observed because degeneracy was lifted by a mixing between states due either to defects or to the contacts. Nevertheless a different experiment [109] displays conductance peaks in clusters of four, indicating that there is a four fold degeneracy (see Fig. 14.*right.bottom* and compare with Fig. 15.*right* where also the temperature dependence according the Beenakker formula is included).

More recently spin states in carbon nanotube quantum dots have been revealed in various systems with the Kondo effect [116–118] and the simple shell structures [119–121]. These experiments allowed a comparison with the predicted

two or four-electron shell structures, depending on the relation between the zero-dimensional level spacing and the subband mismatch. In Ref. [119] low-temperature transport measurements have been carried out on single-wall carbon nanotube quantum dots in a weakly coupled regime in magnetic fields up to 8 Tesla. Four-electron shell filling was observed, and the magnetic field evolution of each Coulomb peak was investigated, in which magnetic field induced spin flip and resulting spin polarization were observed. Excitation spectroscopy measurements have revealed Zeeman splitting of single particle states for one electron in the shell, and demonstrated singlet and triplet states with direct observation of the exchange splitting at zero-magnetic field for two electrons in the shell, the simplest example of the Hund's rule. The total spin in an individual single-wall carbon nanotube quantum dot was also studied in [122] by using the ratio of the saturation currents of the first steps of Coulomb staircases for positive and negative biases. The current ratio reflects the total-spin transition that is increased or decreased when the dot is connected to strongly asymmetric tunnel barriers. The total spin states with and without magnetic fields can be also traced by this method.

**Spin-orbit interaction** Recently also the effects of the Spin-orbit interaction and anomalous spin relaxation was investigated in carbon nanotube quantum dots in order to propose the CN QD as devices for the spintronics. In this sense in a recent papers [123] was shown that the CNT Double Quantum Dot has clear shell structures of both four and eight electrons, with the singlet-triplet qubit present in the four-electron shells. In Ref. [123] the authors observed inelastic co-tunneling via the singlet and triplet states, which they used to probe the splitting between singlet and triplet, in good agreement with theory.

## *Luttinger liquid*

*Transport in 1 Dimension* – Electronic correlations have been predicted to dominate the characteristic features in quasi one dimensional (1D) interacting electron systems. This property, commonly referred to as Tomonaga-Luttinger liquid (TLL or LL) behaviour [124–126], has recently moved into the focus of attention by physicists, also because in recent years several electrical transport experiments for a variety of 1D devices, such as semiconductor quantum wires [127] (QWs) and carbon nanotubes (CNs) [128, 129] have shown this behaviour.

In a 1D electron liquid Landau quasiparticles are unstable and the low-energy excitations take the form of plasmons (collective electron-hole pair modes): this is known as the breakdown of the Fermi liquid picture in 1D. The LL state has two main features: (1) the power-law dependence of physical quantities, such as the tunneling density of states (TDOS), as a function of energy or temperature; (2) the spin-charge separation: an additional electron in the LL decays into decoupled spin and charge wave packets, with different velocities for charge and spin. It follows that 1D electron liquids are characterized by the power-law dependence of some physical quantities as a function of the energy or the temperature. Thus the

tunneling conductance $G$ reflects the power law dependence of the DOS in a small bias experiment [130, 131]

$$G = dI/dV \propto T^{\alpha_{bulk}} \tag{32}$$

for $eV_b = k_B T$, where $V_b$ is the bias voltage, $T$ is the temperature and $k_B$ is Boltzmann′s constant. The exponent $\alpha_{bulk}$ known as *bulk critical exponent*, can be calculated in several different ways as we discuss below.

### The Luttinger Model and the Bosonization Approach

A Tomonaga-Luttinger liquid is a theoretical model describing interacting electrons in a one-dimensional conductor [132–134]. The typical Luttinger model starts from the hypothesis that the Fermi surface consists of two Fermi points, in the neighborhood of which the dispersion curve can be approximated by straight lines with equations

$$\varepsilon_k \approx v_F(|k| - k_F) \equiv v_F \overline{k}. \tag{33}$$

Here we introduce the creation (annihilation) operators for the electrons $\hat{a}^\dagger_{k,s}$ with fixed momentum and spin, and we rewrite the Hamiltonian in Eqs. 28 and 41 in the limit of short range interactions. The scattering processes are usually classified according to the different electrons involved and the coupling strengths labeled with $g$ are often taken as constants. In this case, as discussed in detail by Solyom [132], we can substitute $V^{s,s'}_{k,p}(q)$ with 8 constants (here we limit to 6 ones because we neglect the Umklapp scattering as we explain below). In general we should take into account the dependence on $k, p$ and $q$, however in a model with a bandwidth cut-off, where all momenta are restricted to a small region near the Fermi points, the momentum dependence of the coupling is usually neglected. Thus the kinetic energy takes the form

$$\begin{aligned} H_0 &= v_{\mathrm{F}} \sum_{k,s} \left( (k - k_{\mathrm{F}}) a^\dagger_{+,k,s} a_{+,k,s} + (-k - k_{\mathrm{F}}) a^\dagger_{-,k,s} a_{-,k,s} \right) \\ &= \frac{2\pi v_{\mathrm{F}}}{L} \sum_{q>0,\alpha=\pm,s} \rho_{\alpha,s}(q) \rho_{\alpha,s}(-q), \end{aligned} \tag{34}$$

where density operators for spin projections $s = \uparrow, \downarrow$ have been introduced:

$$\rho_{\pm,s}(q) = \sum_k a^\dagger_{\pm,k+q,s} a_{\pm,k,s}\,. \tag{35}$$

**Interaction** For what concerns the electron-electron interaction, the momentum conservation allows only for four processes, corresponding to $V^{s,s'}_{k,p}(q)$ in Eq. 29:

1. the *Forward Scattering in the same branch*, $g_4^{s,s'}$ for $k$ and $p$ in the same branch and small $q$ (transferred momentum);
2. the *Forward Scattering involving two branches* $g_2^{s,s'}$ for where $k$ and $p$ are opposite and $q$ is small;
3. the *Backward Scattering* ($g_1^{s,s'}$) which involves electrons in opposite branches with large transferred momentum (of order $2k_F$).
4. the *Umklapp scattering* ($g_3^{s,s'}$) additional process significant just at half-filling. Thus in our case we neglect $g_3^{s,s'}$ since the sample is assumed to be doped.

Here we take in account just two types of interaction. First, the "backward scattering" $(k_{\rm F}, s; -k_{\rm F}, t) \rightarrow (-k_{\rm F}, s; k_{\rm F}, t)$ which for $s \neq t$ cannot be rewritten as an effective forward scattering. The corresponding Hamiltonian is

$$H_{\rm int,1} = \frac{1}{L} \sum_{k,p,q,s,t} g_1 a^{\dagger}_{+,k,s} a^{\dagger}_{-,p,t} a_{+,p+2k_{\rm F}+q,t} a_{-,k-2k_{\rm F}-q,s}. \tag{36}$$

And, of course, there is also the forward scattering

$$H_{\rm int,2} = \frac{1}{2L} \sum_{q,\alpha,s,t} \left( g_2(q) \rho_{\alpha,s}(q) \rho_{-\alpha,t}(-q) + g_4(q) \rho_{\alpha,s}(q) \rho_{\alpha,t}(-q) \right). \tag{37}$$

**Exact Solution.** The full Hamiltonian above, $H_0 + H_{int}$ defines the simplest model for interacting electrons in 1D. A simple solvable case is the Tomonaga-Luttinger model [124, 125], where only forward scattering $g_2$ is taken into account ($g_1 = g_3 = g_4 = 0$). It has been solved by Mattis and Lieb [126], who showed that this model describes a particular type of system where the conventional Fermi surface, defined in terms of a step in the momentum distribution, does not exist for arbitrarily small $g_2$. Haldane [135] later extended their analysis to a more general situation and coined the term 'Luttinger liquid' in analogy with the Fermi liquid.

The usual diagonalization of the Tomonaga- Luttinger hamiltonian is based on the so-called bosonization scheme. The density operators $\rho(q)$ act like Bose creation and annihilation operators of elementary excitations with energy $v_F q$ and momentum $q$.

Several important quantities can be exactly calculated for the LL model, including the momentum distribution function [126] and various response functions [132], which generally exhibit power-law behavior [134, 136, 137].

All properties of a TL liquid can be described in terms of only two effective parameters per degree of freedom which take over in 1D the role of the Landau parameters familiar from Fermi liquid theory.

In particular the low-energy properties of a homogeneous 1D electron system could be completely specified by the TL coefficients corresponding to the interaction ($g_i^{s,\sigma}$) and the kinetic energy ($v_F$) in the limit of ideal TL liquid.

Four TL parameters, depending on $g$ and $v_F$, characterize the low energy properties of interacting spinful electrons moving in one channel: the parameter $K_\nu$ fixes the exponents for most of the power laws and $v_\nu$ is the velocity of the long wavelength excitations: $\nu = \rho$ for the charge and $\nu = \sigma$ for the spin. The parameters [138] $K_\rho$ and $v_{\rho/\sigma}$ are easily obtained as functions of $g_i^{s,\sigma}$ and $v_F$ by various techniques found in textbooks [132].

$$K_\nu = \sqrt{\frac{\pi v_F + g_4^\nu - g_2^\nu}{\pi v_F + g_4^\nu + g_2^\nu}} \tag{38}$$

$$v_\nu = \sqrt{\left[v_F + \frac{g_4^\nu}{\pi}\right]^2 - \left(\frac{g_2^\nu}{\pi}\right)^2} \tag{39}$$

$$\alpha = \frac{1}{2}\left[\left(v_F + \frac{g_4^\sigma}{\pi}\right)\frac{1}{v_\sigma} + \left(v_F + \frac{g_4^\rho}{\pi}\right)\frac{1}{v_\rho} - 2\right] \tag{40}$$

where $g_i^\sigma = \frac{1}{2}(g_i^p - g_i^\perp)$ and $g_i^\rho = \frac{1}{2}(g_i^9 + g_i^\perp)$. Here $\alpha$ denotes the *bulk* critical exponent which characterizes many properties of the transport behaviour of a 1D device (e.g. the zero bias conductance as a function of $T\backslash,$). Notice that $g_4$ leads to a small renormalization of the Fermi velocity, which is usually neglected.

The model described above, with linear branches and constant interaction in momentum space is known as TL model and corresponds to a very short range interaction (Dirac delta). The presence of a long range interaction in a 1D electron system introduces in the model an infrared divergence and is quite difficult to solve. Next we discuss the solutions for the case of Carbon Nanotubes obtained with a Renormalization Group approach and a Dimensional Crossover.

### Low-Energy Theory for Correlated Carbon Nanotubes

A formal description of the LL in CNs was developed at the end of 1990s because CNs display complex quasi-1D characteristics, which are required to reconsider and extend the basics of LL theory. In fact in CNs the Fermi surface is described by four points of the Brillouin zone, instead of the two points found for a single channel. Moreover the transport properties of a CN depend also on the diameter and chirality. Thus the LL theory was first developed for a metallic armchair SWCN [139]. There the low-energy theory including Coulomb interactions is derived and analyzed. It describes two fermion chains without interchain hopping but coupled in a specific way by the interaction. The strong-coupling properties were studied by bosonization, and consequences for experiments on single armchair nanotubes were discussed.

The electronic properties of carbon nanotubes are due to the special bandstructure of the $\pi$ electrons in graphite [25, 27] as we discussed in Sect. “Electronic Structure of Single-Wall Nanotubes”. The Fermi surface for a metallic CN, obtained starting from Eq. 10, consists of two distinct Fermi points $\alpha K$ with $\alpha = \pm$. As usually

here the $y$-axis points along the tube direction and the circumferential variable is $0 \leq \phi \leq 2\pi$. As we discussed above since the basis of graphite contains two carbon atoms, there are two sublattices $p = \pm$ shifted by the vector $\vec{d} = (0, d)$, and hence two degenerate Bloch states at each Fermi point $\alpha K_s$. The quantization of transverse motion gives the 'mass' $m_{eff}$[26], according the Dirac fermions approach, which vanishes for the lowest subband of a metallic CN.

Because the excitation of other transversal bands costs energy, the bandwidth cutoff scale $D$ we take in account just the lowest subband in the limit of linear dispersion as shown in Fig. (12.*left*). Thus, the non interacting part of Hamiltonian is a massless 1D Dirac Hamiltonian [26, 27]

$$H_0 = -v \sum_{p\alpha\sigma} p \int dy \; \psi^{\dagger}_{p\alpha\sigma} \partial_y \psi_{-p\alpha\sigma} \; . \tag{41}$$

**Electron electron interaction.** In order to introduce electron electron repulsion we have to introduce the Coulomb interactions mediated by a screened potential. Thus we start from the unscreened Coulomb repulsion$(a_0; a)$ in a wrapped 2D geometry

$$V_0(y - y', \varphi - \varphi') = \frac{e^2/\kappa}{\sqrt{(y - y')^2 + 4R^2 \sin^2(\varphi - \varphi')}}. \tag{42}$$

The Fourier transform $\hat{V}_0(q)$ reads

$$\hat{V}_0(q) \approx \frac{e^2/\kappa}{\sqrt{2}} \left[ K_0\left(\frac{qR}{2}\right) I_0\left(\frac{qR}{2}\right) \right]. \tag{43}$$

Here the effects of electrons trapped in nonpropagating orbitals were incorporated in terms of a dielectric constant $\kappa$, $K_0(q)$ denotes the modified Bessel function of the second kind, $I_0(q)$ is the modified Bessel function of the first kind. The nanotube radius $R$ yields a natural Ultra Violet (UV) cutoff (for $q \approx \frac{2\pi}{R}$) of the interaction.

We can also define a 1D potential $V_0$ (the 1D limit of the complete interaction) and the corresponding Fourier transform $V_0(k)$ for $|kR| = 1$,

$$V_0(y) = \frac{2e^2}{\kappa\pi\sqrt{a_0^2 + y^2 + 4R^2}} K\left(\frac{2R}{\sqrt{a_0^2 + y^2 + 4R^2}}\right);$$

$$V_0(k) = \frac{e^2}{\kappa} \left[2|\ln(kR)| + \pi \ln 2\right]. \tag{44}$$

with the complete elliptic integral of the first kind $K(z)$.

**Scattering processes** Thus we rewrite the coefficients $g_i^{\alpha}$ written for the short range interaction in Fourier transform by analyzing the scattering processes allowed for a CN. Thus we now distinguish four processes associated with the Fermi points $\alpha = \pm$:

1. the 'forward scattering' ($\alpha$FS) where $\alpha_1 = \alpha_4$ and $\alpha_2 = \alpha_3$
2. the 'backscattering' ($\alpha$BS) with $\alpha_1 = -\alpha_2 = \alpha_3 = -\alpha_4$ while
3. at half-filling there could be an additional 'Umklapp' process ($\alpha$US) characterized by $\alpha_1 = \alpha_2 = -\alpha_3 = -\alpha_4$ which we neglect in what follows.
4. In CNs an additional 'Forward scattering' term ($f$) which measures the difference between intra- and inter-sublattice interactions, can be introduced following [139, 140]. This term is due to the hard core of the Coulomb interaction. i.e. it follows from the unscreened short range component of the interaction.

These processes are different from the conventional ones discussed above since they do not necessarily mix right- and left-moving branches but rather involve different Fermi points.

**Forward Scattering** The $\alpha$FS interaction couples only the total 1D charge densities,

$$H^{(0)}_{\alpha \mathrm{FS}} = \frac{1}{2} \int dy dy' \, \rho(y) V_0(y - y') \rho(y') \, , \tag{45}$$

with $\rho(y) = \sum_{p\alpha\sigma} \psi^{\dagger}_{p\alpha\sigma} \psi_{p\alpha\sigma}$. If we now introduce an infra red cut off given by the CN′s length, $L$ as $k \geq q_c = \frac{2\pi}{L}$ we can define $g_2 \approx V_0(q_c)$.

Obviously the continuum argument (used obtaining $V(q)$ as a Fourier Transform in Eq. 29) plays for $|x| >> a$ while for $|x| \leq a$, an additional FS term arises due to the hard core of the Coulomb interaction,

$$H^{(1)}_{\alpha \mathrm{FS}} = -f \int dx \sum_{p\alpha' \sigma\sigma'} \psi^{\dagger}_{p\alpha\sigma} \psi^{\dagger}_{-p\alpha'\sigma'} \psi_{-p\alpha'\sigma'} \psi_{p\alpha\sigma} \tag{46}$$

with $f/a = \gamma e^2/R$. Evaluating $f$ on the wrapped graphite lattice yields

$$\gamma = \frac{\sqrt{3}a}{2\pi\kappa a_0} \left[ 1 - \frac{1}{\sqrt{1 + a^2/3a_0^2}} \right] \approx 0.1 \, . \tag{47}$$

This process was not analyzed in term of the $g_i$ in the LL classical approach. In the language of a Hubbard model, we have $f/a = U - V$ where $U = e^2/R$ is the on-site and $V$ the nearest-neighbor Coulomb interaction. According to Eq. 47, this difference is small compared to $U$.

**Backward scattering.** Thus we discuss $\alpha$BS contributions. Since the discussed Fourier Transform involves a rapidly oscillating factor $\exp[2iK_x(x - x')]$, these are local processes which do not resolve sublattices,

$$H_{\alpha BS} = \frac{b}{2}\int dy \sum_{pp'\alpha\sigma\sigma'} \psi^{\dagger}_{p\alpha\sigma}\psi^{\dagger}_{p'-\alpha\sigma'}\psi_{p'\alpha\sigma'}\psi_{p-\alpha\sigma} \ . \tag{48}$$

Estimating the coupling constant we obtain $b \approx f$, while for well-screened short-ranged interactions, one has $b >> f$. In terms of $g_i$ we have $b = g_1 = V_0(2K_s)$.

**Bulk Critical exponent in CNs.** For this LL model in the metallic armchair tube, a single interaction parameter, $g$,

$$\frac{1}{g} = K = \sqrt{1 + \frac{g_2}{(2\pi v_F)}} \approx \sqrt{1 + \frac{U_0(q_c)}{(2\pi v_F)}},$$

will drive the power-law temperature-dependent for eV $= k_BT$ and voltage-dependent for eV $= k_BT$ tunneling conductances.

Thus the critical exponent can be written in terms of $g$ as

$$\alpha_{bulk} = \frac{1}{4}\left(g + 1/g - 2\right), \tag{49}$$

which depends just on the forward scattering part of the interaction. Here $U_0$ can be read as the charging energy, whereas $v_F h/2L$ is the single-particle level spacing. The charging energy follows from the capacitive properties of the metal-nanotube junction and from the electronic structure, so that no universal value can be derived.

Accordingly, the low-temperature conductance $dI/dV \propto V^{\alpha_{bulk}}$, while the linear conductance becomes $G(T) \propto T^{\alpha_{bulk}}$.

The conductance suppression at low temperature or bias has been shown to become even more dramatic for tunneling into the end of a long nanotube, with an exponent that we will calculate in a following section.

In order to estimate the value of the critical exponent we can follow the calculation of Egger and Gogolin [139, 141], where was obtained

$$g = \left\{1 + \frac{8e^2}{\pi\kappa\hbar v}[ln(L/2\pi R) + 0.51]\right\}^{-1/2}. \tag{50}$$

Thus, $g$ is a function of the interaction strength and $g < 1$ corresponds to a repulsive interaction. In the experiments [129], bulk tunneling was measured fitting the high-temperature data, $\alpha \approx 0.34$ corresponding to a value of $g \approx 0.22$, in agreement with theoretical estimates [139, 140, 142].

**Multi-wall carbon nanotubes and doping.** The low-energy theory for multi-wall carbon nanotubes including the long-ranged Coulomb interactions, internal screening effects, and single-electron hopping between graphite shells was derived and analyzed by bosonization methods. Characteristic Luttinger liquid power laws are found for the tunneling density of states, with exponents approaching their Fermi liquid value only very slowly as the number of conducting shells, N, increases.

The bulk critical exponent was calculated by using bosonization techniques [143] and was obtained

$$\alpha_{bulk} \approx \frac{1}{4N}\left(K_N + \frac{1}{K_N} - 2\right), \tag{51}$$

where

$$\frac{1}{K_N} \approx \sqrt{1 + \frac{NU_0(q_c)}{(2\pi v_F)}}.$$

Afterwards the tunneling density of states of doped multiwall nanotubes including disorder and electron-electron interactions was computed and a non-conventional bahaviour was found [144]. In Ref. [144] this behaviour was explained in terms of a particularly effective and non-conventional Coulomb blockade (CB) for tunneling into a strongly interacting disordered metal.

The discussed explanation in terms of conducting shells does not agree with the measurements of the conductance which usually refer to the outer layer,also if the electronic properties are influenced by the interaction with inner metallic cylinders. Moreover MWNTs use to be significantly doped, which leads to the presence of a large number of subbands at the Fermi level [152] (see Fig. 16.*left*). Thus the number $N$ in Eq. 51 is often assumed to be the number of subbands crossing the Fermi level.

The contribution of a large number of modes at low energies has then an appreciable impact on the enhancement of observables like the tunneling density of states. This issue is relevant for the investigation of the nanotubes of large radius that are present in the MWNTs, which may have a large $N$. Experiments reported in [153], where measurements of the tunneling conductance have been carried out in doped MWNTs, with a number of subbands at the Fermi level $N \approx 10 - 20$ (in the outer layer).

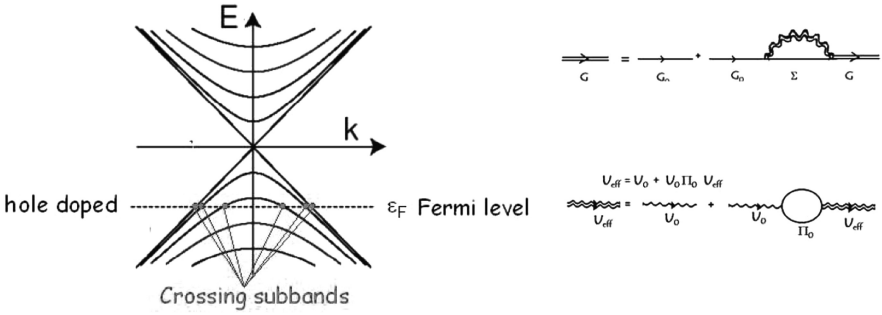


**Fig. 16** The degree of doping in CNTs corresponds to the position of the Fermi energy. From a measurement of the conductance as a function of a gate voltage, which shifts the Fermi energy, we can argue the doping level. Nanotubes can be turned to n-type semiconducting by potassium Doping in a Vacuum, Vacuum Annealing or Electrostatic Doping while re-exposure to air reverts NT to p-type [145]. In fact several groups have concluded that charge transfer from oxygen to the nanotube leads to p-doping [146–149] while n-doping can be obtained by direct doping of the tube with an electropositive element such as potassium [150, 151]. In MWNTs the experimental conditions refer to a situation where $N_s = 5:10$ and the suppression of tunnelling in MWNT can be softened by increasing the doping level

We conclude that by doping carbon nanotubes it is possible to alter significantly the electronic, mechanical and chemical properties of the tubes.

## *RG Approach to the Luttinger Liquid*

In Refs. [154–158], was introduced a Renormalization group (RG) method, in order to study the low-energy behaviour of the unscreened e–e repulsion in CNs. In some of these papers a dimensional regularization approach was presented, useful, when dealing with effects of the long-range Coulomb interaction. As we discuss below this method allows to avoid the infrared singularities arising from the long-range Coulomb interaction at $D = 1$.

### Generalized Interaction

From the theoretical point of view, a relevant question is the determination of the effects of the long-range Coulomb interaction in CNs. It is known that the Coulomb interaction is not screened in one spatial dimension [159], although usually the e–e interaction is taken actually as short-range (TL model). Thus a dimensional regularization approach [160] was developed in order to analyze the low energy effects of the divergent long-range Coulomb interaction in one dimension. The interaction potential in arbitrary dimensions now reads

$$U_D(r-r') = \int_0^{2\pi}\int_0^{2\pi} \frac{c_D d\varphi d\varphi'}{4\pi^2|\bar{r}-\bar{r}'|} u_0(\varphi,k)\, u_0(\varphi,p)\, u_0\left(\varphi',(k+q)\right) u_0\left(\varphi',(p-q)\right) = \frac{c_D}{|r-r'|}. \tag{52}$$

Here $r$ is a vector in the $D$ dimensional space and $\bar{r}$ is a vector in $D+1$ dimensions.

As it is known, the Coulomb potential $1/|r|$ can be represented in three spatial dimensions as the Fourier transform of the propagator $1/k^2$

$$\frac{1}{|r|} = \int \frac{d^3k}{(2\pi)^3} e^{ik\cdot r}\, \frac{1}{k^2}. \tag{53}$$

If the interaction is projected onto one spatial dimension, by integrating for instance the modes in the transverse dimensions, then the Fourier transform has the usual logarithmic dependence on the momentum [154]. We choose instead to integrate formally a number $3 - D$ of dimensions, so that the long-range potential gets the representation

$$\frac{1}{|x|} = \int \frac{d^Dk}{(2\pi)^D} e^{ikx}\, \frac{c(D)}{|k|^{D-1}}, \tag{54}$$

where $c(D) = \Gamma((D-1)/2)/(2\sqrt{\pi})^{3-D}$.

**RG Solution for D=1**

The starting Hamiltonian for the interacting 1D system is analogous to the sum of Eqs. 41 and 45,

$$H = \int_0^{\Lambda} \frac{dp}{(2\pi)} \psi^+(p)\varepsilon(p)\psi(p) + \int_0^{\Lambda} \frac{dp}{(2\pi)}\ \rho(p)\ U_0(p)\ \rho(-p) \tag{55}$$

where $\rho(p)$ are density operators made of the electron modes $\psi(p)$, and $U_0(p)$ corresponds to the Fourier transform of the 1D interaction potential. Here it also present an Ultra Violet cut-off, $\Lambda$, that can be estimated as the order of the bandwidth $D$.

In writing Eq. 55, were neglected backscattering processes that connect the two branches of the dispersion relation. This is justified, in a first approximation, as for the Coulomb interaction the processes with small momentum transfer have a much larger strength than those with momentum transfer $\approx 2k_F$. The backscattering processes give rise, however, to a marginal interaction.

The one-loop polarizability $\Pi_0(k, \omega_k)$ is given by the sum of particle-hole contributions within each branch

$$\Pi_0(k, \omega_k) = \frac{v_F k^2}{|v_F^2 k^2 - \omega_k^2|}\ . \tag{56}$$

The effective interaction is found by the Dyson equation (see Fig. 16.*right*)

$$U_{\mathit{eff}}(k, \omega_k) = \frac{U_0(k)}{1 - U_0(k)\Pi_0(k, \omega_k)}, \tag{57}$$

so that the self-energy follows: $\Sigma_{\mathit{eff}} = G_0 U_{\mathit{eff}} = G_0 U_{\mathit{eff}} = \frac{G_0 U_0}{1 - U_0 \Pi_0}$.

In the spirit of the GW approximation, $v_F$ can be assumed as a free parameter that has to match the Fermi velocity in the fermion propagator after self-energy corrections.

The polarization gives the effective interaction $U_{\mathit{eff}}$ as in Eq. 57 which incorporates the effect of plasmons in the model. We compute the electron self-energy by replacing the Coulomb potential by the effective interaction

$$\begin{aligned} i\Sigma(k, i\omega_k) =& i\frac{e^2}{2\pi} \int_{-E_c}^{E_c} \frac{dp}{2\pi} \int_{-\infty}^{+\infty} \frac{d\omega_p}{2\pi} \frac{1}{i(\omega_p + \omega_k) - v_F(p + k)} \\ & \frac{U_0(p)}{1 - \dfrac{e^2}{\pi} \dfrac{v_F p^2}{v_F^2 p^2 + \omega_p^2} U_0(p)}. \end{aligned} \tag{58}$$

This approximation reproduces the exact anomalous dimension of the electron field in the Luttinger model with a conventional short-range interaction [157]. The only contributions in (58) depending on the bandwidth cutoff are terms linear in $\omega_k$ an $k$. There is no infrared catastrophe at $\omega_k \approx v_F k$, because of the correction in the slope

of the plasmon dispersion relation, with respect to its bare value $v_F$. The result that we get for the renormalized electron propagator is

$$G^{-1}(k,\omega_k) = Z_\Psi^{-1}\,(\omega_k - v_F k) - \Sigma(k,\omega_k)$$

$$\approx Z_\Psi^{-1}\,(\omega_k - v_F k) + Z_\Psi^{-1}\,(\omega_k - v_F k)\int \frac{dp}{|p|}\frac{(1-f(p))^2}{2\sqrt{f(p)}\left(1+\sqrt{f(p)}\right)^2} + \ldots, \quad (59)$$

where $f(p) \equiv 1 + U_0(p,\omega_c)/(2\pi v_F)$ and $Z_\Psi^{1/2}$ is the scale of the bare electron field compared to that of the cutoff-independent electron field

$$\Psi_{bare}(E_c) = Z_\Psi^{1/2}\Psi\ . \quad (60)$$

The first RG flow equations, obtained analogously to the more general Eq. 67 obtained below, becomes

$$E_c\frac{d}{dE_c}\,\log\,Z_\Psi(E_c) = \frac{\left(1-\sqrt{f(E_c)}\right)^2}{8\sqrt{f(E_c)}}. \quad (61)$$

As it is known [156], the critical exponent can be easily obtained from the right side of Eq. 61 in the limit of $\log(E_c) \to 0$. If we assume $U(q)$ as a constant, $g_2$, it results

$$\sqrt{f(q)} = \sqrt{1+\frac{g_2}{(2\pi v_F)}} = K.$$

However as we discussed above the forward scattering involves small momentum transferred, $q$, thus if we suppose $q = q_c$ ($q \to q_c$ is a limit for the natural infrared cutoff), we obtain $g_2 = U(q_c)$. Hence, as it is clear from a comparison with Eqs. 49 and 61,

$$\alpha_Z = \frac{\left(1-\sqrt{f(q_c)}\right)^2}{8\sqrt{f(q_c)}} = \frac{1}{4}\left(K + \frac{1}{K} - 2\right).$$

**Dimensional Regularization Near D=1**

A different approach was proposed in [155], where was developed an analytic continuation in the number of dimensions, in order to regularize the infrared singularity of the long-range Coulomb interaction at $D = 1$ [161]. The aim of this approach was to find the effective interaction between the low-energy modes of CNs, which have quite linear branches near the top of the subbands ($K_S$). For this purpose it needs to introduce the analytic continuation to a general dimension $D$ of the linear dispersion around each Fermi point, i.e. the Hamiltonian

$$H = v_F \sum_{\alpha\sigma} \int_0^\Lambda dp|p|^{D-1} \int \frac{d\Omega}{(2\pi)^D}\ \psi^+_{\alpha\sigma}(p)\,\sigma\cdot p\ \psi_{\alpha\sigma}(p) + e^2 \int_0^\Lambda dp|p|^{D-1} \int \frac{d\Omega}{(2\pi)^D}\ \rho(p)\ \frac{c(D)}{|p|^{D-1}}\ \rho(-p), \tag{62}$$

where the $\sigma_i$ matrices are defined formally by $\{\sigma_i, \sigma_j\} = 2\delta_{ij}$. Here $\rho(p)$ are density operators made of the electron modes $\psi_{\alpha\sigma}(p)$, and $c(D)/|p|^{D-1}$ corresponds to the Fourier transform of the Coulomb potential in dimension $D$. Its usual logarithmic dependence on $|p|$ at $D = 1$ is obtained by taking the 1D limit with $c(D) = \Gamma((D-1)/2)/(2\sqrt{\pi})^{3-D}$.

A self-consistent solution of the low-energy effective theory has been found in [154, 155, 162] by determining the fixed-points of the RG transformations implemented by the reduction of the cutoff $\Lambda$. The Renormalization Group theory with a dimensional crossover starts from Anderson suggestion [163] that the Luttinger model could be extended to 2D systems. The dimensional regularization approach of Refs. [154, 155, 162] overcomes the problem of introducing such an external parameter.

A phenomenological solution of the model was firstly obtained [154, 155, 162], carrying a dependence on the transverse scale needed to define the 1D logarithmic potential, which led to scale-dependent critical exponents and prevented a proper scaling behavior of the model [154, 155, 162, 164].

The long-range Coulomb interaction may lead to the breakdown of the Fermi liquid behavior at any dimension between $D = 1$ and $D = 2$, while the CN description lies between that of a pure 1D system and the 2D graphite layer. Then an analytic continuation is introduced in the number $D$ of dimensions which allows to carry out the calculations needed, in order to accomplish the renormalization of the long-range Coulomb interaction at $D \to 1$.

In the vicinity of $D = 1$, a crossover takes place to a behavior with a sharp reduction of the electron quasiparticle weight and the DOS displays an effective power-law behavior, with an increasingly large exponent. For values of $D$ above the crossover dimension, a clear signature of quasiparticles at low energies is obtained and the DOS approaches the well-known behavior of the graphite layer.

As in the previous section the one-loop polarizability $\Pi_0(k, \omega_k)$ is given by the sum of particle-hole contributions within each branch. Now it is the analytic continuation of the known result in Eq. 56, which we take away from $D = 1$, in order to carry out a consistent regularization of the Coulomb interaction

$$\Pi_0(k, \omega_k) = b(D) \frac{v_F^{2-D} k^2}{|v_F^2 k^2 - \omega_k^2|^{(3-D)/2}}, \tag{63}$$

where $b(D) = \frac{2}{\sqrt{\pi}} \frac{\Gamma((D+1)/2)^2 \Gamma((3-D)/2)}{(2\sqrt{\pi})^D \Gamma(D+1)}$. The effective interaction is found by the Dyson equation in Eq. 57, so that the self-energy $\Sigma_{eff}$ follows. After dressing

the interaction with the polarization (63), the electron self-energy is given by the expression

$$\Sigma(k,\omega_k) = -e^2 \int_0^{E_c/v_F} dp|p|^{D-1} \int \frac{d\Omega}{(2\pi)^D} \int \frac{d\omega_p}{2\pi} G(k-p,\omega_k-\omega_p) \frac{-i}{\frac{|p|^{D-1}}{c(D)} + e^2\Pi(p,\omega_p)}. \quad (64)$$

At general $D$, the self-energy (64) shows a logarithmic dependence on the cutoff at small frequency $\omega_k$ and small momentum $k$. This is the signature of the renormalization of the electron field scale and the Fermi velocity. In the low-energy theory with high-energy modes integrated out, the electron propagator becomes

$$\frac{1}{G} = \frac{1}{G_0} - \Sigma \approx Z^{-1}(\omega_k - v_F\ \sigma\ \cdot k) - Z^{-1} f(D) \sum_{n=0}^{\infty} (-1)^n g^{n+1} \left( \frac{n(3-D)}{n(3-D)+2} \omega_k + \left(1 - \frac{2}{D} \frac{n(3-D)+1}{n(3-D)+2}\right) v_F\ \sigma\ \cdot k \right) h_n(D) \log(\Lambda), \quad (65)$$

where $g = (2b(D)c(D)e^2)/v_F$, $f(D) = \dfrac{1}{2^D \pi^{(D+1)/2} \Gamma(D/2) b(D)}$ and $h_n(D) = \dfrac{\Gamma(n(3-D)/2 + 1/2)}{\Gamma(n(3-D)/2+1)}$. The quantity $Z^{1/2}$ represents the scale of the bare electron field compared to that of the renormalized electron field for which $G$ is computed.

The effective coupling $g$ is a function of the cut off with an initial value obtained carrying out an expansion near $D = 1$ [156],

$$g_0(D) = c(D)\frac{e^2}{v_F} \approx \frac{e^2}{\pi^2 v_F} \frac{1}{D-1}. \quad (66)$$

The renormalized propagator $G$ must be cutoff-independent, as it leads to observable quantities in the quantum theory. This condition is enforced by fixing the dependence of the effective parameters $Z$ and $v_F$ on $\Lambda$, as more states are integrated out from high-energy shells. We get the differential renormalization group equations

$$\Lambda \frac{d}{d\Lambda} \log Z(\Lambda) = -f(D) \sum_{n=0}^{\infty} \frac{n(3-D)(-g)^{n+1}}{n(3-D)+2} h_n(D) = -\gamma(g), \quad (67)$$

$$\Lambda \frac{d}{d\Lambda} g(\Lambda) = -f(D) \frac{2(D-1)}{D} g^2 \sum_{n=0}^{\infty} (-g)^n \frac{(3-D)n+1}{(3-D)n+2} h_n(D) = -\beta(g). \quad (68)$$

For $D = 1$ the function in the r.h.s. of Eq. 68 vanishes, so that the 1D model has formally a line of fixed-points, as it happens in the case of short-range interaction. In the crossover approach shown in this section, the effective coupling $g$ is sent to strong coupling in the limit $D \to 1$, and the behavior of the RG flow in this regime

remains to be checked. The dependence on $D$ of the functions appearing in the RG equations shows itself in the form of $D-1$ and $D-3$ factors, revealing that these are the two critical dimensions, corresponding to a marginal and a renormalizable theory, respectively.

In order to approach the limit $D \to 1$, we have to look for the asymptotic dependence on $D$ of the functions appearing in the RG equations. We will see that this dependence appears as $D-1$ and $D-3$ factors, revealing that these are the two critical dimensions, corresponding to a marginal and a renormalizable theory, respectively.

Starting with the function $\beta(g)$, we need to carry out the sum at the right-hand-side of Eq. 67. This is given in terms of the hypergeometric special functions [156]. However the $\beta$ function near $D=1$ can be approximated with the simple function of $g$ and $d$ to first order in $D-1$,

$$\beta(g) \approx -\frac{f(D)}{4}\frac{2(D-1)}{D}\sqrt{\pi}g\left(1-\frac{1}{\sqrt{1+g}}\right). \tag{69}$$

The $\gamma$ function can be expressed in the form

$$\gamma(g) = \frac{f(D)}{4}\frac{3-D}{2}gT_D(g) \tag{70}$$

where the series $T_D(g)$ is available on tables. For $D=1$ it has the simple expression

$$T_1(g) = \sqrt{\pi}\frac{2\sqrt{g+1}-g-2}{g\sqrt{g+1}} \tag{71}$$

The scaling of the electron wave function near $D=1$ is therefore given by

$$\gamma(g) \approx \frac{f(D)}{4}\sqrt{\pi}\left(2-\sqrt{1+g}-\frac{1}{\sqrt{1+g}}\right) \tag{72}$$

This coincides formally with the anomalous dimension that is found at $D=1$ in the exact solution of the Luttinger model, what provides an independent check of our RG approach to the 1D system.

The dimensional crossover approach allows to calculate the critical exponent also in the case of a divergent interaction for $D \to 1$. The DOS computed at dimensions between 1 and 2 displays an effective power-law behavior which is given by $n(\varepsilon) : Z(\varepsilon)|\varepsilon|^{D-1}$, for several dimensions approaching $D=1$. Then by introducing the low-energy behavior of $Z(\varepsilon)$ in order to analyze the linear dependence of $\log(n(\varepsilon))$ on $x=-\log(\Lambda)$ it can be obtained

$$\log(n(\varepsilon)) \approx \log Z(\varepsilon) + (D-1)\log(|\varepsilon|) \approx (\alpha_Z - (D-1))\,x \equiv \alpha_D x. \tag{73}$$

Here $\alpha_Z$ can be easily written starting from Eq. 67, if we limit ourselves to a simple first order expansion near $x = 0$ with $(\log(Z) \approx \gamma(g_0)x)$, where $g_0$ is the initial value of the coupling (see Eq. 66)

$$\alpha_Z \approx T_1(\sqrt{1+g_0})g_0\frac{(3-D)f(D)(D+1)}{8}. \tag{74}$$

The analytic continuation in the number of dimensions allows to avoid the infrared singularities that the long-range Coulomb interaction produces at $D = 1$, providing insight, at the same time, about the fixed-points and universality classes of the theory in the limit $D \to 1$.

In order to compare the results of this approach with experiments, as in [156], a lower bound for the exponent of the DOS can be obtained by estimating the minimum of the absolute value of $\alpha_D$, for dimensions ranging between $D = 1$ and $D = 2$. The evaluation can be carried out starting from Eqs. 73 and 74. A minimum value for $|\alpha_D|$ as a function of $D$, by introducing the expression of $g_0(D)$ in Eq. 66, was obtained. From Fig. 17 we can see that the maximum value for $\alpha_D$ $(\alpha_M)$ corresponds to a dimension between 1 and 1.2. If the number of subbands is increased, then the value of $|\alpha_M|$ decreases while the corresponding dimension approaches 1.

**Doping in Multi Wall Carbon Nanotubes.** In the case of doped MWNTs the effect of having a number $N$ of subbands crossing the Fermi level, which multiply consequently the number of electron fields and terms in the hamiltonian has to be

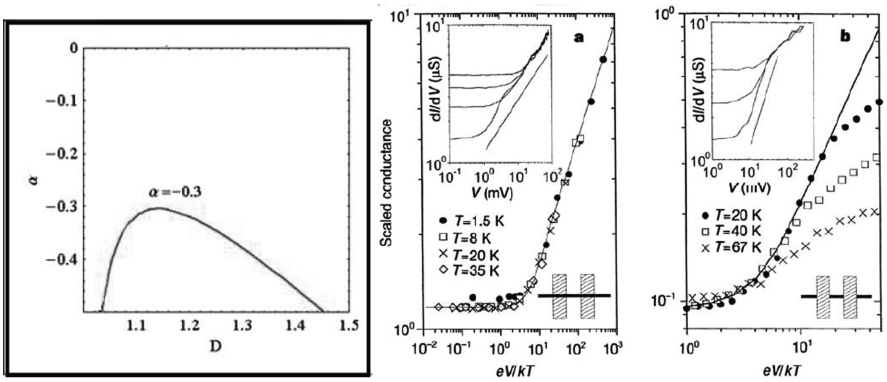


**Fig. 17** (*Left*) $\alpha$ as a function of the dimension, and we choose the maximum value of this function between $D = 1$ and $D = 2$ as an estimate of the critical exponent. We find a value for $\alpha$ in the usual undoped nanotube that reproduces the anomalous exponent measured experimentally ($\alpha \approx -0.3$), corresponding to a dimension for the crossover between 1.1 and 1.2. (*Right*) Inset in a, dI/dV curves taken on a bulk-contacted rope at temperatures T = 1.6 K, 8 K, 20 K and 35 K. Inset in b, dI/dV curves taken on an end-contacted rope at temperatures T = 20 K, 40 K and 67 K. In both insets, a straight line on the log–log plot is shown as a guide to the eye to indicate power-law behaviour. The main panels a and b show these measurements collapsed onto a single curve by using the scaling relations described in the text. The solid line is the theoretical result fitted to the data by using as a fitting parameter. The values of resulting in the best fit to the data are = 0.46 in a and = 0.63 in b. From [165]

incorporated. Thus the analytic continuation to general dimension $D$ of the one loop polarizability becomes

$$\Pi(k,\omega_k) = 2Nb(D)\frac{v_F^{2-D}k^2}{|v_F^2k^2-\omega_k^2|^{(3-D)/2}}. \tag{75}$$

The equations presented above have to be rewritten by including the number of subbands so that $\alpha_D$ in Eq. 73 becomes

$$\alpha_D \approx g_0 T_1(g_0)\frac{(3-D)f(D)(D+1)}{8\,N} - (D-1). \tag{76}$$

In [156] was obtained, in the limit of large $N$ and small values of $D-1$,

$$\alpha_Z \approx -\frac{f(D)(3-D)(D+1)}{8\,N}\sqrt{\pi\, g_0}, \tag{77}$$

and was obtained that $\alpha_Z$ vanishes at large $N$ as : $1/\sqrt{N}$, and it diverges at $D \to 1$ as $1/\sqrt{D-1}$.

## Results and Experiments

### *Experimental Evidence of LL Behavior*

In the last decade several transport and photoemission studies provided evidence for the existence of the TLL state in CNs. In these studies, power-law behavior of temperature and bias dependent conductivity and a power-law Fermi edge was observed, respectively.

The non-Ohmic behavior of the conductance at low bias voltage, the so called zero-bias anomaly (ZBA), is a clear signature of a tunneling contact between a Fermi liquid and a strongly correlated system. Thus evidence of LL behavior in CNs has been found in many experiments [129, 165], where a measurement of the temperature dependence of the resistance was carried out, above a crossover temperature $T_c$[166]. In Fig. 16.*right* are reported measurements of the conductance of bundles ('ropes') of SWNTs as a function of temperature and voltage that agree with predictions for tunnelling into a Luttinger liquid. In particular, we find that the conductance and differential conductance scale as power laws with respect to temperature and bias voltage, respectively, and that the functional forms and the exponents are in good agreement with theoretical predictions [165]. In these experiments (e.g. [129]), bulk tunnelling was measured fitting the high-temperature data, $\alpha \approx 0.34$ corresponding to a value of $g \approx 0.22$, in agreement with with theoretical estimates [139, 156].

Power-law conductance behavior with exponent values in the range of theoretical predictions was also found for crossed metallic junctions of SWNTs [167], giving confidence in the manifestation of a Luttinger liquid state in small-diameter SWNTs.

Alternatively, by means of angle-integrated photoemission measurements of SWNTs, some power-law behavior of the spectral function and intensities was also found to be in good agreement with LL model predictions [168].

Also the Nuclear magnetic resonance (NMR) can be a powerful method to characterize correlated states of materials as it is sensitive to the density of states near the Fermi edge. Recently experiments by Singer et al. [169] showed a deviation from Fermi-liquid behavior in carbon nanotubes with an energy gap evident at low temperatures.

**Effects of Doping.** The effect of doping was taken in account in [152]. There was explored the electric-field effect of carbon nanotubes (NTs) in electrolytes. Due to the large gate capacitance, Fermi energy shifts of order $\pm 1V$ can be induced, enabling to tune NTs from p to n-type. Consequently, large resistance changes are measured. The measurements of a power law behaviour were also carried out in the MWNTs by studying the tunneling of electrons into the CN. Nanotube/electrode interfaces with low transparency as well as nanotube/nanotube junctions created with atomic force microscope manipulation have been used. The tunneling conductance goes to zero as the temperature and bias are reduced, and the functional form is consistent with a power law suppression of tunneling as a function of energy. The exponent depends upon sample geometry. It has been reported that the values of the critical exponent $\alpha_{bulk}$ measured in 11 different samples range from 0.24 to 0.37 [153].

This variation can be accounted for within the RG approach reported above by assuming that a large number of subbands, $N_s$ is involved (N = 2 to N = 10). Thus the effect of doping was studied in the suppression of tunneling observed in MWNTs, incorporating as well the influence of the finite dimensions of the system. The scaling approach reported above allowed to encompass the different values of the critical exponent measured for the tunneling density of states in carbon nanotubes. Thus was predicted that further reduction of $\alpha_{bulk}$ should be observed in multiwalled nanotubes with a sizeable amount of doping.

From a theoretical point of view, in the case of nanotubes with a very large radius, was found a pronounced crossover between a high-energy regime with persistent quasiparticles and a low-energy regime with the properties of a one-dimensional conductor.

**Magnetic field effects on Luttinger Liquid behaviour.** The effects of a transverse magnetic field $B$, acting on CNs were also investigated in the last years. Theoretically, it is predicted that a perpendicular $B$ field modifies the DOS of a CN [40], leading to the Landau level formation as we discussed above. In a recent letter Kanda et al. [170] examined the dependence of $G$ on perpendicular $B$ fields in MWNTs (see Fig. 18). They found that, in most cases, $G$ is smaller for higher magnetic fields, while $\alpha_{Bulk}$ is reduced by a factor $1/3$ to $1/10$, for $B$ ranging from 0 to 4 T. Following the calculation proposed for a semiconducting quantum Wire [32] the effects of transverse magnetic field were analyzed in large radius CNs [157]. The presence of $B \neq 0$ produces the rescaling of all repulsive terms of the interaction between electrons, with a strong reduction of the backward scattering, due to the edge localization of the electrons. Our results imply a variation with $B$ in the value

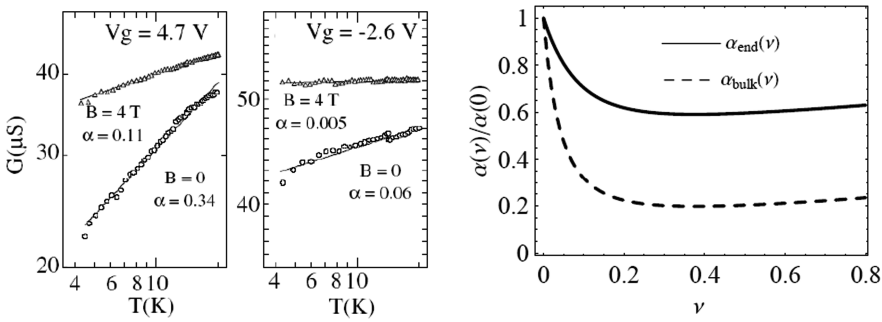


**Fig. 18** (*Left*) Perpendicular magnetic field dependence of the $G - T$ data for two gate voltages $V_g = 4.7\text{V}$ (**a**), and 2.6V (**b**). In both cases, the data follow the power-law behavior, and the exponent depends on the magnetic field (from [170]. Critical exponents versus the magnetic field dependent parameter, $\nu$, for a large radius CN: $\alpha_{bulk}$ is calculated following Eq. 51, $\alpha_{end}$ is calculated following Eq. 79. The magnetic field rescales the values of the Fermi velocity and the strength of e–e interaction. It follows that the effects of a transverse magnetic field also involve the value of $K$. Thus, we predict a reduction of the critical exponents $\alpha_{bulk}$ and $\alpha_{end}$, by giving magnetic field dependent exponents for the power law behaviour of the conductance

of $\alpha_{Bulk}$, which is in fair agreement with the value observed in transport experiments [170].

In order to obtain the critical exponent it is possible to calculate $U_0(q, \omega_c)$ starting from the eigenfunctions $\Psi_{0,k_F}(\varphi, y)$ and the potential in Eq. 42. We focus our attention on the forward scattering (FS) terms. We can obtain $g_2$, FS between opposite branches, corresponding to the interaction between electrons with opposite momenta, $\pm k_F$, with a small momentum transfer $\approx q_c$. The strength of this term reads

$$g_2 = U_0(q_c, B, k_F, -k_F)$$

$$= \frac{c_0}{N_2(\nu)}\left[K_0\left(\frac{q_c R}{2}\right) I_0\left(\frac{q_c R}{2}\right) + u_2(\nu) K_1\left(\frac{q_c R}{2}\right) I_1\left(\frac{q_c R}{2}\right)\right],$$

where $K_n(q)$ denotes the modified Bessel function of the second kind, $I_n(q)$ is the modified Bessel function of the first kind, while $N_2$ and $u_2$ are functions of the transverse magnetic field, as was discuss in the appendix of [171].

By introducing into Eq. 51 the calculated values of $g_2$ and $g_4$, it follows that the bulk critical exponent is reduced by the presence of a magnetic field, as we show in Fig. 18.

## *Intramolecular Devices*

**Impurity.** Since 1995 intramolecular devices have also been proposed which should display a range of other device functions [172–177]. For example, by introducing

a pentagon and a heptagon into the hexagonal carbon lattice, two tube segments with different atomic and electronic structures can be seamlessly fused together to create intramolecular metal–metal, metal–semiconductor, or semiconductor–semiconductor junctions. Electrical transport SWNTs with intramolecular junctions was measured and was demonstrated that a metal–semiconductor junction behaves like a rectifying diode with nonlinear transport characteristics. In the case of a metal–metal junction, the conductance appears to be strongly suppressed and it displays a power-law dependence on temperatures and applied voltage, consistent with tunneling between the ends of two Luttinger liquids [129].

From a theoretical point of view the power-law behaviour characterizes also the thermal dependence of $G$ when an impurity is present along the 1D devices. The theoretical approach to the presence of obstacles mixes two theories corresponding to the single particle scattering (by a potential barrier $V_B(r)$) and the TLL theory of interacting electrons. The single particle scattering gives the transmission, probability, $|t|^2$, depending in general on the single particle energy $\varepsilon$. Hence, following [134, 136], the conductance, $G$, as a function of the temperature and $|t|$ can be obtained

$$G \propto |t(\varepsilon, T)|^2 \equiv |t(\varepsilon)|^2 T^{2\alpha_{end}}, \tag{78}$$

where we introduced a second critical exponent [171], $\alpha_{end}$

$$\alpha_{end} \approx \frac{1}{2}\left(\frac{1}{K} - 1\right). \tag{79}$$

The results obtained in [129] agreed with theoretical prediction.

**Intrinsic Quantum Dot.** Experiments [178, 179] show transport through an intrinsic quantum dot (QD) formed by a double barrier within a 1D electron system, allowing for the study of the resonant or sequential tunneling. The linear conductance typically displays a sequence of peaks, when the gate voltage, $V_g$, increases. Thus also the double-barrier problem has attracted a significant amount of attention among theorists [180–187], in particular for the case of two identical, weakly scattering barriers at a distance $d$. In general, the transmission is non-zero for particular values of the parameters corresponding to a momentum $k_F$, such that $\cos(k_F d/2) = 0$. It follows that, although in a 1D electron system for repulsive interaction the conductance is suppressed at zero temperature by the presence of one impurity (1D metal becomes a perfect insulator), the presence of an intrinsic QD gives rise to some peaks in the conductance at $T = 0$ corresponding to the perfect transmission. This *resonant scattering* condition corresponds to an average particle number between the two barriers of the form $\nu + 1/2$, with integer $\nu$, i.e. the "island" between the two barriers is in a degenerate state. If interactions between the electrons in the island are included, one can recover the physics of the Coulomb blockade [188].

The power-law behaviour characterizes also the thermal dependence of $G$ in the presence of an IQD. A first theory about the transport through an IQD is known as *Uncorrelated Sequential Tunneling* (UST), where an incoherent sequential

tunneling is predicted. It follows the dependence of the peaks of the conductance according to the power law

$$G_{max} \propto T^{\alpha_{end}-1}.$$

However in order to explain the unconventional power-law dependencies in the measured transport properties of a CN [178, 179], a different mechanism was proposed [178, 183], namely, *correlated sequential tunneling* (CST) through the island. The temperature dependence of the maximum $G_{max}$ of the conductance peak, according to the CST theory, yields the power law behaviour

$$G_{max} \propto T^{\alpha_{end-end}-1} = T^{2\alpha_{end}-1}. \tag{80}$$

Recently a lot of theoretical work has been carried out on the double impurity problem in TLL systems. In an intermediate temperature range $\varepsilon_c << k_B T << \Delta_{dot}$, where $\varepsilon_c$ is the Infra Red cut-off energy and $\Delta_{dot}$ is the level spacing of the dot, some authors [184, 185] predict a behaviour according to the UST, while others [187] find results in agreement with the CST theory. In a recent paper [189] the authors discussed how the critical exponent can depend on the size of the dot and on the temperature, by identifying three different regimes, i.e. the UST at low $T$, a Kirchoff regime at intermediate $T$ ($G_{max} \propto T^{2\alpha_{end}}$) and a third regime for $T >> \Delta_{dot}$, with $G_{max} \propto T^{-1}$. Thus, in their calculations, obtained starting from spinless fermions on the lattice model, no evidence of CST is present.

Then, the problem of the transport through a Quantum Dot formed by two intramolecular tunneling barriers along the MWNT, weakly coupled to Tomonaga-Luttinger liquids is studied, including the action of a strong transverse magnetic field $B$. There were predicted [30] the presence of some peaks in the conductance G versus $B$, related to the magnetic flux quantization in the ballistic regime (at a very low temperature, $T$) and also at higher $T$, where the Luttinger behaviour dominates. The temperature dependence of the maximum $G_{max}$ of the conductance peak according to the Sequential Tunneling follows a power law, $G \propto T^{\gamma_e - 1}$ with $\gamma_e$ linearly dependent on the critical exponent, $\alpha_{end}$, strongly reduced by $B$ as shown in Fig. 18.*right*.

## *Intermediate Regimes and Crossover*

**Crossover from Luttinger liquid to Coulomb Blockade regime.** Now we discuss the experimental data reported in a recent letter by Kanda et al. [170], in which the intermediate regime has been explored measuring the zero-bias conductance at temperatures where the thermal energy becomes comparable to the level spacing in the discrete single-particle spectrum. In Ref. [170] the authors have reported a systematic study of the gate voltage dependence of the LL-like behaviour in MWNTs, showing the dependence of the exponent $\alpha$ on gate voltage, with values of $\alpha$ ranging from 0.05 to 0.35. The main results of [170] are as follows:

1. the gate-voltage ($V_g$) dependence of the exponent $\alpha$ below 30 K exhibits periodic oscillations; the characteristic $V_g$ scale for $\alpha$ variation, $\Delta V_g$, is around 1 V;
2. changes in the exponent $\alpha$ are observed in the plots of the conductance at an inflection temperature $T^* \approx 30$ K, for values of $V_g$ corresponding to peaks of $\alpha$.

In their letter, Kanda et al. do not find plausible the explanation of the mentioned features starting from a LL description of the MWNTs. In this respect, Egger has considered in [143] a model for MWNTs composed of a number $N_{SH}$ of ballistic metallic shells. The author has discussed there a low-energy theory for the MWNTs including long-ranged Coulomb interactions and internal screening effects. The theory may be also extended to include the effect of a variable number of conducting modes modulated by the doping level. However, Kanda et al. rule out the possibility that the change in the number of subbands at the Fermi level may be at the origin of the features observed in their experiment, as long as the subband spacing is too large to be consistent with the period of the oscillations.

Then, Kanda et al. turn to a different kind of theory that considers the MWNT as a diffusive conductor. Egger and Gogolin [144] have calculated the TDOS of doped MWNTs including disorder (with mean free path $l$ smaller than the radius $R$) and electron-electron interactions. MWNTs may display an effective and nonconventional CB arising from tunneling into a strongly interacting disordered metal, leading to LL-like zero-bias anomalies: the exponent becomes $\alpha = (R/2\pi\hbar D\nu_0)\log(1+\nu_0 U)$, where $D$ is the diffusion constant, $\nu_0 = N_s/2\pi\hbar v_F$ is the noninteracting density of states depending on the number of subbands $N_s$ and the Fermi velocity $v_F$, and $U_0$ is an effectively short-ranged 1D interaction. Substituting these parameters by pertinent values yields an estimate $\alpha$; $R/N_s l$, that is near the experimentally observed values.

Kanda and coworkers conclude that this second theory better explains the experimental results, by assuming that the mean-free path $l$ may fluctuate with the gate voltage. This is based on the theoretical work by Choi et al. [190], that have studied the effects of single defects on the local density of states via resonant backscattering. However, the argument of Kanda et al. has not addressed the question of how a random distribution of defects may produce the oscillations observed in the experiment. We believe otherwise that the dependence of the $\alpha$ exponent on the gate voltage is in correspondence with a definite periodic structure of the single-particle density of states.

A theoretical approach was developed in [191, 192] to the low-energy properties of 1D electron systems aimed to encompass the mixed features of Luttinger liquid and Coulomb blockade behavior observed in the crossover between the two regimes. For this aim the Luttinger liquid description was extended by incorporating the effects of a discrete single-particle spectrum. The intermediate regime is characterized by a power-law behavior of the conductance, but with an exponent oscillating with the gate voltage, in agreement with recent experimental observations. This construction also accounts naturally for the existence of a crossover in the zero-bias conductance, mediating between two temperature ranges where the power-law behavior is preserved but with different exponent.

**Crossover from Fabry-Perot to Coulomb Blockade regime.** For good contact, the SWCNT acts as an electron wave guide creating resonances at certain energies and can be regarded as an open quantum dot with the resonances corresponding to the broad energy levels. As we discussed above in the opposite limit (CB regime) of very low transparency, the electrons are forced to tunnel one by one and the energy levels sharpens due to their longer life time.

An intermediate regime also exists in which the electron number on the dot is still fixed but significant cotunneling is allowed. This leads to different kinds of Kondo effects related to the total excess spin [193–195] and/or the orbital degree of freedom on the SWCNT quantum dot [196, 197].

The transition between these regimes was reported in [198] where the authors discussed how transport evolves from being wave-like transmission known as Fabry-Perot interference to single particle-like tunneling of electrons or holes. In the intermediate regime four Coulomb blockade peaks appear in each Fabry-Perot resonance, which is interpreted as entering the SU(4) Kondo regime. A bias shift of opposite polarity for the Kondo resonances for one electron and one hole in a shell is in some cases observed.

## Superconducting Transition

The Superconductivity behaviour in low dimensional systems is a quite interesting question since 40 years ago Mermin and Wagner [199] proved a famous theorem stating that it is impossible for abrupt phase transitions with long-range order to occur in 1- or 2-D systems at finite temperature. Thus CNs are among the best candidates for investigating the possibility of (quasi)1D superconductivity. In general CNs do not show superconducting properties but some recent experiments found that they can can superconduct by showing also high superconducting transition temperature, $T_c \approx 10°$ K. [200, 201].

### *Experimental Evidence of Superconductivity in CNs*

The field of SC in nanotubes started experimentally with the discovery of a strong proximity-induced SC in isolated or bundled SWNTs connected to superconducting leads [202, 203]. Proximity-induced superconductivity in single-walled carbon nanotubes below 1° both in a single tube 1 nm in diameter and in crystalline ropes containing about 100 nanotubes, was observed [202]. In these experiments, the CNs were assumed to be in the normal, $N$, state but with a phase coherence length $L_\phi$ and a thermal length $L_T$ larger than the superconducting coherence length, allowing for the *SNS* junction to sustain a very high supercurrent below the lead transition temperature.

Measurements on ropes of single-walled carbon nanotubes (SWNT) in low-resistance contact to non-superconducting (normal) metallic pads were reported in [204]. It was found a 2 orders of magnitude resistance drop below 0.55°K, which

is destroyed by a magnetic field of the order of 1 T, or by a dc current greater than 2.5 μA. These features suggested the existence of intrinsic superconductivity in ropes of SWNT. Then in Ref. [205] were reported low-temperature transport measurements on suspended single-walled carbon nanotubes (both individual tubes and ropes) that indicated the presence of attractive interactions in carbon nanotubes which overcome Coulomb repulsive interactions at low temperature, and enabled investigation of superconductivity in a one-dimensional limit never explored before.

In 2001, ultra-small-diameter single wall nanotubes (USCN), with diameter of $\approx$ 0.4 nm, have been produced inside the channels of a zeolite matrix. Possible metallic geometries compatible with such a small radius are the armchair (3, 3) and the zig-zag (5, 0) ones. The ultra-small diameter of these tubes induces many unusual properties, such as a superconducting transition temperature $T_c \approx 15°\mathrm{K}$ [200], much larger than that observed in bundles of larger diameter tubes [204].

In MWNTs, where disorder and impurities can play a central role, supercurrents have been even harder to achieve. Enhanced conductance was observed near zero bias, which was interpreted in terms of multiple Andreev reflections in the presence of inelastic processes [206]. On the other hand, proximity induced supercurrent has been observed [207] also in an individual, diffusive MWNT using bulk(side)-contacted samples with Ti/Al contacts [208].

In Ref. [201] it was reported that there is a superconducting phase in entirely end-bonded MWNTs with a transition temperature $T_c \approx 12°\mathrm{K}$. The TEM images showed a MWNT with an outer diameter of $2R_o = 7.4$ nm, and inner diameter of $2R_i < 2$ nm ($R < 1$ nm) while the emergence of this superconductivity is highly sensitive to the junction structures of the Au electrode/MWNTs and $T_c$ depends on the numbers of electrically activated shells.

More recently a gradual magnetization drop with an onset temperature (Tc) of 18 23 K has been found in the honeycomb arrays of multiwalled CNTs (MWNTs) showing a slight resistance decrease due to superconductivity [209]. The disappearance of the Meissner effect after destroying the array structure suggested that intertube coupling of MWNTs in the honeycomb array is a dominant factor for the mechanism.

## *Theoretical Approach*

The superconducting phase in 1D systems enters into competition with another type of quantum order, the charge-density-wave (CDW) phase, an instability very specific to 1D systems (while the SC one occurs irrespective of the dimension).

While the SC transition induces the creation or destruction of electron (Cooper) pairs, the CDW is induced by the spontaneous formation of electron-hole excitations.

### The Phase Diagram and Breakdown of a Luttinger Liquid

Effective field theory was solved in practically exact way by Egger and Gogolin [139]. As we discussed above, they analyzed a (10, 10) SWNT, next $CN_{10}$. Thus

they showed that both $g_1$ and $f$ scale as $1/R$ and in $CN_{10}$ they are much smaller than $g_2$ [139] but at low temperature their effects should be included. In [139] this has been realized by means of a renormalization group calculation. The main result is the existence of two different crossover temperatures, namely

$$kT_f = De^{-\frac{2\pi v_F}{f}} \quad \text{and} \quad kT_b = De^{-\frac{2\pi v_F}{g_1}}$$

associated to the dominance of $f$ and $g_1$ respectively. Below these temperatures the Luttinger liquid breaks down and a (quasi-) long-range order phase appears. Thus the presence of a SC phase due to the effect of the short range $g_1$ and $f$ was predicted, but at very low temperatures ($T_b \approx 0.1$ m°K and $T_f \leq T_b$).

This behaviour can be summarized in the phase diagram reported in Fig. 19. Calculations for a $CN_{10}$ predict that 1D superconductivity is the dominant instability only at $T < 1$ m°K with screened interactions thus a purely electronic mechanism is not sufficient. Moreover for long-ranged interactions (which is the case of nanotubes in typical conditions), we have $T_f \approx T_b$, while for short-ranged interactions it results $T_f < T_b$. In the latter case a superconducting instabilty is predicted at $T \approx T_f$ if the Luttinger liquid parameter $g$ is larger than $1/2$.

Starting from these results a pure electronic mechanism which gives Superconductivity needs:

i) Screening of the forward scattering, $g_2$ (long range effect $g > 0.5$)
ii) Increasing of the backward scattering, $g_1$ (short range effect $T_b$)
iii) Relevant effects from the lattice (high value of the corresponding temperature, $T_f$)

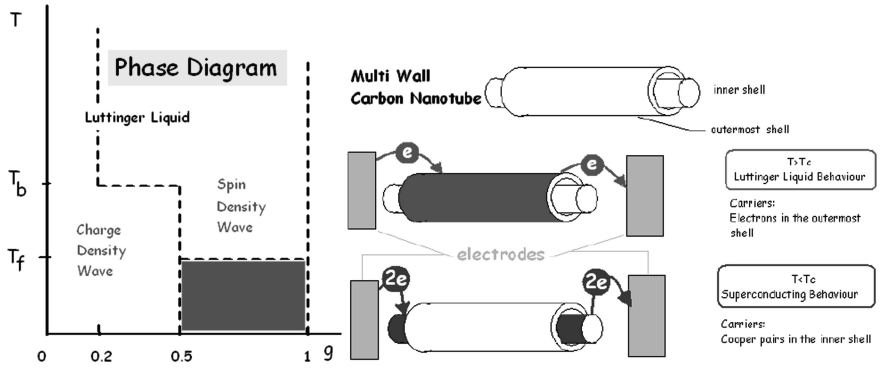


**Fig. 19** The transition temperature for $CN_{10}$ with the typical long-range interaction is estimated to be $T_f : T_b : 1$ mK, i.e. a value certainly hard to be observed. This is due to the smallness of $g_1$ and $f$ (compared to $g_2$), since they scale as $1/R$ and are sizeable only for very thin tubes. (*left*) We assume that all shells of an entirely end bonded MWNT are resistors in a parallel connection. For $T > T_c$ the current is due to the flow of electrons in the outermost shells with the typical behaviour of a Luttinger Liquid. For $T < T_c$ a superconducting transition is allowed in the innermost shell; thus the transport is due to Cooper pairs

### Some Phonon Based Theories

Many studies about the electron-phonon interaction focused on isolated tubes and in particular on the possible occurrence of a Peierls instability [210]. Such an instability is always expected to occur in 1D systems. Thus the coupling to long-wavelength acoustic modes such as twistons or radial breathing modes (derived from the transverse acoustic modes of graphite) was studied as a means to induce a CDW instability.

**Superconductivity in carbon nanotube ropes** – In order to explain superconductivity in the experiment of [205] was derived and analyzed the low-energy theory of superconductivity in carbon nanotube ropes [211]. The rope was modelled as an array of metallic nanotubes, taking into account phonon-mediated as well as Coulomb interactions, and arbitrary Cooper pair hopping amplitudes between different tubes. Quantum phase slips are shown to cause a depression of the critical temperature Tc below the mean-field value, and a temperature-dependent resistance below $T_c$. Thus was found a signature of the presence of attractive phonon-mediated interactions in carbon nanotubes, which can even overcome the repulsive Coulomb interactions [212].

According Ref. [213], the critical supercurrents found in experiments on the proximity effect of [202] can be explained by the presence of a short-range attractive interaction coming from the coupling to the elastic modes of the nanotube. In a further letter [214], the autor discussed the strong suppression of single-particle hopping between neighboring nanotubes in a disordered rope and conclude that the tunneling takes place in pairs of electrons, which are formed within each nanotube due to the existence of large superconducting correlations. Thus a model was developed to account that the single-particle hopping between neighboring nanotubes in a rope is strongly suppressed [215] because the different helical structure of the nanotubes leads to the misalignment of their lattices.

Thus the effect of superconductivity does not rely exclusively on the properties of the individual nanotubes in agreement with the discussed priciple that any correlation in a 1D system can only develop a divergence at zero temperature [216]. Moreover was demonstrated [217] that the interaction among a large number of metallic nanotubes favors the appearance of a metallic phase in the ropes, intermediate between respective phases with spin-density-wave and superconducting correlations. These arise in samples with about 100 metallic nanotubes or more, where the long-range Coulomb interaction is very effectively reduced and it may be overcome by the attractive interaction from the exchange of optical phonons within each nanotube.

Later were introduced the renormalization of intratube interactions and the effect of intertube Coulomb screening. Thanks to this aproach was possible to study both the limits of thin and thick ropes ranging from purely one-dimensional physics to the setting of 3D Cooper-pair coherence [218].

**Superconductivity in small-diameter carbon nanotubes.** The SC and instablities were investigated in CNs of small radius in order to explain the results of [200]. According to [219] the Luttinger liquid behavior breaks down in the undoped (3, 3)

nanotubes at low temperatures, due to the appearance of soft modes in the sector of current excitations. The instabilities that may lead to the breakdown of the Luttinger liquid in the small-diameter (5, 0) nanotubes were analyzed in [219]. There the authors focused on the competition between the effective interaction mediated by phonon exchange and the Coulomb interaction also by analyzing the effects of screening.

The softening of phonons by electron-phonon interactions and the Peierls transition was also studied in the specific case of small tubes [220, 221]. The increase of the coupling with radius was shown to lead to a Peierls distortion at several hundred Kelvin mediated by $2k_F$ phonons in the (3, 3) armchair case [220, 221].

**Electronic instabilities of doped multi-walled nanotubes.** In doped multi-walled nanotubes each shell has in general a manifold of Fermi points, thus an analysis based on the scale dependence of the different scattering processes, showed that a pairing instability arises for a large enough number of Fermi points as a consequence of their particular geometric arrangement. The instability is enhanced by the tunneling of Cooper pairs between nearest shells, giving rise to a transition from the Luttinger liquid to a superconducting state in a wide region of the phase diagram [222].

**Isolated Single wall nanotube.** Thus most of the studyes concluded that the sorrounding environment plays a central role on the SC transition of a CN. Thus in isolated nanotubes, Coulomb repulsion should easily overcome the attractive interaction mediated by phonons. However in [223], using a one-loop renormalization group method the authors concluded that a SC order may dominate in the (5, 0) tube provided that the electron-phonon interaction is strong enough. Moreover a possible dominant triplet-state superconducting instability was suggested to arise from the specific three-band topology at the Fermi level of isolated (5, 0) tubes [224].

### Other Theories

A different mechanism of carbon nanotube superconductivity that originates from edge states which are specific to graphene was proposed in [225]. Using on-site and boundary deformation potentials which do not cause bulk superconductivity, was obtained an appreciable transition temperature for the edge state.

In Ref. [226] the issue was discussed, whether a superconducting behavior in small radius carbon nanotubes can arise by a purely electronic mechanism by a comparison between two different approaches, (1) the first one based on the Luttinger Model, (2) the second one, which emphasizes the role of the lattice and short range interaction, developed starting from the Hubbard Hamiltonian. By using the latter model a transition temperature of the same order of magnitude as the measured one was predicted.

By a Luttinger liquid-like approach, one finds enhanced superconducting correlations due to the strong screening of the long-range part of the Coulomb repulsion. It was shown that the presence of many nanotubes inside the zeolite matrix of the experiment in [200] provides a strong screening of the long range component of the electron-electron interaction ($g_2$), mainly due to the presence of electronic currents

in neighboring nanotubes, while the short range components ($f$ and $g_1$) have to remain almost unchanged.

This allows for the occurrence of a sizable superconducting instability within the Luttinger liquid approach. Based on this finding, the autors performed a detailed analysis on the resulting Hubbard-like model, and calculated transition temperatures of the same order of magnitude as the measured ones [226].

In the experiment of [201] the authors claim that almost all the shells of the MWNTs are electrically active. Such a high quality of the contacts seems to be crucial, in order to observe the superconducting transition at such a high temperature. Moreover the clear power-law of the conductance observed for $T > T_c$ is consistent with the Luttinger liquid character of the normal state. Therefore the observed sharp breakdown of the power-law at $T_c$ is an indication that an approach based on the superconducting instability of the Luttinger liquid is well posed.

Moreover, as we discussed above, in a typical transport experiment, only the outermost shell of the MWNT becomes electrically active. As a consequence the conducting channel is not efficiently screened and retains a strong 1D character. On the other hand, the activation of the internal shells gives a large dielectric effect, due to intra- and inter-shell screening, and at the same time it provides an incipient 3D character, which is crucial for establishing the superconducting coherence.

In Ref. [227], as reported in Fig. 19, all contacted shells can carry the normal current as resistors in parallel connection and at $T > T_c$, the electrons flow in each shell. It is however clear that the conductance $G$ is mainly given by the outermost shells, because they have more conducting channels due to larger radius. For what concerns $T < T_c$, the theory predicts that superconductivity is favored in the inner part of the MWNT, where the radius of the shells is reduced, in particular, in the innermost shell which is able to support the transport of Cooper pairs. This scenario is in line with the prediction [228, 229] of an increase in pair binding energy with decreasing nanotube radius.

Notice that both the doping and the screening of long-range part of the electron-electron repulsion, needed to allow the SC phase, are related to the intrinsically 3D nature of the environment where the CNs operate [230].

**Acknowledgments** This work was supported in part by the EU under the 7th Framework Program ICT-2007.8.1 FET Proactive 1: Nano-scale ICT devices and systems Carbon nanotube technology for high-speed next-generation nano-Interconnects (CATHERINE) project, Grant Agreement n. 216215.

## References

1. S. Iijima, Helical microtubules of graphitic carbon. Nature **354**, 56 (1991)
2. P.L. McEuen, Carbon-based electronics. Nature **393**, 15 (1998)
3. A. Oberlin, M. Endo, T. Koyama, Filamentous growth of carbon through benzene decomposition. J. Cryst. Growth **32**, 335–349 (1976)
4. H.W. Kroto, J.R. Heath, S.C. O'Brien, R.F. Curl, R.E. Smalley, $C_{60}$:Buckminsterfullerene. Nature **355**, 162–163 (1985)
5. T.W. Ebbesen, Carbon nanotubes. Phys. Today **49**(6), 26 (1996)

6. R.E. Smalley, Discovering the fullerenes. Rev. Mod. Phys. **69**, 723 (1997)
7. P.G. Collins, A. Zettl, H. Bando, A. Thess, R.E. Smalley, Nanotube nanodevice. Science **278**, 100 (1997)
8. A. Thess, R. Lee, P. Nikolaev, H. Dai, P. Petit, J. Robert, C. Xu, Y.H. Lee, S.G. Kim, A.G. Rinzler, D.T. Colbert, G. Scuseria, D. Tománek, J.E. Fischer, R.E. Smalley, Crystalline ropes of metallic carbon nanotubes. Science **273**, 483 (1996)
9. G. Gao, T. Cagin, W.A. Goddard III., Energetics, structure, mechanical and vibrational properties of single walled carbon nanotubes (SWNT). Nanotechnology **9**, 184–191 (1998)
10. M. Motta, Y.L. Li, I. Kinloch, A. Windle, Mechanical properties of continuously spun fibers of carbon nanotubes. Nano Lett. **5**(8), 1529–1533 (2005)
11. A.A. Puretzky, H. Schittenhelm, X.D. Fan, M.J. Lance, L.F. Allard, D.B. Geohegan, Investigations of single-wall carbon nanotube growth by time-restricted laser vaporization. Phys. Rev. B **65**(24), 245425 (2002)
12. P.X. Hou, S.T. Xu, Z. Ying, Q.H. Yang, C. Liu, H.M. Cheng, Hydrogen adsorption/desorption behavior of multi-walled carbon nanotubes with different diameters. Carbon **41**(13), 2471–2476 (2003)
13. R. Saito, G. Dresselhaus, M.S. Dresselhaus, *Physical Properties of Carbon Nanotubes* (Imperial College Press, London, 1998)
14. J. González, F. Guinea, M.A.H. Vozmediano, The electronic spectrum of fullerenes from the Dirac equation. Nucl. Phys. B **406**, 771 (1993)
15. A.H. Castro Neto, F. Guinea, N.M.R. Peres, K.S. Novoselov, A.K. Geim, The electronic properties of graphene. Rev. Mod. Phys. **81**, 109–162 (2008)
16. K.S. Novoselov, A.K. Geim, S.V. Morozov, D. Jiang, Y. Zhang, S.V. Dubonos, I.V. Gregorieva, A.A. Firsov, Electric field effect in atomically thin carbon films. Science **306**, 666 (2004)
17. A.H. Castro Neto, F. Guinea, N.M.R. Peres, Drawing conclusions from grapheme. Phys. World **19**, 33 (2006)
18. M.I. Katsnelson, K.S. Novoselov, A.K. Geim, Chiral tunnelling and the Klein paradox in grapheme. Nat. Phys. **2**, 620 (2006)
19. M.I. Katsnelson, K.S. Novoselov, Graphene: New bridge between condensed matter physics and quantum electrodynamics. Solid State Commun. **143**, 3 (2007)
20. N.M.R. Peres, F. Guinea, A.H. Castro Neto, Electronic properties of disordered two-dimensional carbon. Phys. Rev. B **73**, 125411 (2006)
21. V.P. Gusynin, S.G. Sharapov, Unconventional integer quantum hall effect in graphene. Phys. Rev. Lett. **95**, 146801 (2005)
22. K.S. Novoselov, A.K. Geim, S.V. Morozov, D. Jiang, M.I. Katsnelson, I.V. Grigorieva, S.V. Dubonos, A.A. Firsov, Two dimensional gas of massless Dirac fermions in graphene. Nature **438**, 197 (2005)
23. Y. Zhang, Y.-W. Tan, H.L. Stormer, P. Kim, Experimental observation of the quantum Hall effect and Berry's phase in graphene. Nature **438**, 201 (2005)
24. S. Reich, J. Maultzsch, C. Thomsen, P. Ordejón, Tight-binding description of grapheme. Phys. Rev. B **66**, 035412 (2002)
25. P.R. Wallace, The band theory of graphite. Phys. Rev. **71**, 622 (1947)
26. C.L. Kane, E.J. Mele, Size, Shape, and low energy electronic structure of carbon nanotubes. Phys. Rev. Lett. **78**, 1932 (1997)
27. D.P. Di Vincenzo, E.J. Mele, Self-consistent effective-mass theory for intralayer screening in graphite intercalation compounds. Phys. Rev. B **29**, 1685 (1984)
28. H.-W. Lee, D.S. Novikov, Supersymmetry in carbon nanotubes in a transverse magnetic field. Phys. Rev. B **68**, 155402 (2003)
29. X. Zhou, J.-Y. Park, S. Huang, J. Liu, P.L. McEuen, Band structure, phonon scattering, and the performance limit of single-walled carbon nanotube transistors. Phys. Rev. Lett. **95**, 146805 (2005)

30. S. Bellucci, P. Onorato, Transport through a double barrier in large radius carbon Nanotubes in the presence of a transverse magnetic field. Eur. Phys. J. B **52**, 469–476 (2006)
31. T. Ando, T. Seri, Quantum transport in carbon nanotubes in magnetic fields. J. Phys. Soc. Jpn. **66**, 3558 (1997)
32. S. Bellucci, P. Onorato, Transport through a double barrier for interacting quasi one-dimensional electrons in a quantum wire in the presence of a transverse magnetic field. Eur. Phys. J. B **45**, 87–96 (2005)
33. J.P. Lu, Novel magnetic properties of carbon nanotubes. Phys. Rev. Lett. **74**, 1123 (1995)
34. R. Saito, G. Dresselhaus, M.S. Dresselhaus, Erratum: Magnetic energy bands of carbon nanotubes. Phys. Rev. B **53**, 10408 (1996)
35. S. Bellucci, J. Gonzalez, F. Guinea, P. Onorato, E. Perfetto, Magnetic field effects in carbon nanotubes. J. Phys. Condens. Matter **19** 395017 (2007)
36. E. Perfetto, J. Gonzalez, F. Guinea, S. Bellucci, P. Onorato, Quantum hall effect in carbon nanotubes and curved grapheme strips. Phys. Rev. B **76**, 125430 (2007)
37. N. Nemec, G. Cuniberti, Phys. Rev. B **74**, 165411 (2006)
38. M.F. Lin, K.W.-K. Shung, Magnetoconductance of carbon nanotubes. Phys. Rev. B **51**, 7592 (1995)
39. W. Tian, S. Datta, Aharonov-Bohm-type effect in graphene tubules: A Landauer approach. Phys. Rev. B **49**, 5097 (1994)
40. H. Aiki, T. Ando, Electronic states of carbon nanotubes. J. Phys. Soc. Jpn. **62**, 1255 (1993)
41. H. Ajiki, T. Ando, Energy bands of carbon nanotubes in magnetic fields. J. Phys. Soc. Jpn. **65**, 505 (1996)
42. J.-O. Lee, J.-R. Kim, J.-J. Kim, J. Kim, N. Kim, J. W. Park, K.-H. Yoo, Observation of magnetic-field-modulated energy gap in carbon nanotubes. Solid State Commun. **115**, 467 (2000)
43. A. Rochefort, P. Avouris, F. Lesage, D.R. Salahub, Electrical and mechanical properties of distorted carbon nanotubes. Phys. Rev. B **60**, 13824 (1999)
44. M.S.C. Mazzoni, H. Chacham, Bandgap closure of a flattened semiconductor carbon nanotube: A first-principles study. Appl. Phys. Lett. **76**, 1561 (2000)
45. P.E. Lammert, P.H. Zhang, V.H. Crespi, Gapping by squashing: Metal-insulator and insulator-metal transitions in collapsed carbon nanotubes. Phys. Rev. Lett. **84**, 2453 (2000)
46. Ç. Kılıç, S. Ciraci, O. Gülseren, T. Yildirim, Variable and reversible quantum structures on a single carbon nanotube. Phys. Rev. B **62**, 16345 (2000)
47. M.T. Figge, M. Mostovoy, J. Knoester, Peierls transition with acoustic phonons and solitwistons in carbon nanotubes. Phys. Rev. Lett. **86**, 4572 (2001)
48. X. Zhou, H. Chen, O.-Y. Zhong-can, Can electric field induced energy gaps in metallic carbon nanotubes? J. Phys. Condens. Mattter **13**, L635 (2001)
49. D.S. Novikov, L.S. Levitov, Energy anomaly and polarizability of carbon nanotubes. Phys. Rev. Lett. **96**, 036402 (2006)
50. J. Jiang, J. Dong, D.Y. Xing, Zeeman effect on the electronic spectral properties of carbon nanotubes in an axial magnetic field. Phys. Rev. B **62**, 13209 (2000)
51. S. Roche, G. Dresselhaus, M.S. Dresselhaus, R. Saito, Aharonov-Bohm spectral features and coherence lengths in carbon nanotubes. Phys. Rev. B **62**, 16092 (2000)
52. F.L. Shyu, C.P. Chang, R.B. Chen, C.W. Chiu, M.F. Lin, Magnetoelectronic and optical properties of carbon nanotubes. Phys. Rev. B **67**, 045405 (2003)
53. Y. Aharonov, D. Bohm, Significance of electromagnetic potentials in the quantum theory. Phys. Rev. **115**, 485 (1959)
54. R.A. Webb, S. Washburn, C.P. Umbach, R.B. Laibowitz, Observation of *h*/*e* Aharonov-Bohm oscillations in normal-metal rings. Phys. Rev. Lett. **54**, 2696 (1985)
55. A. Bachtold, C. Strunk, J.-P. Salvetat, J.-M. Bonard, L. Forro, T. Nussbaumer, C. Schönenberger, Aharonov-Bohm oscillations in carbon nanotubes. Nature (London) **397**, 673 (1999)

56. B. Lassagne, J-P. Cleuziou, S. Nanot, W. Escoffier, R. Avriller, S. Roche, L. Forro, B. Raquet, J.-M Broto, Aharonov-Bohm conductance modulation in ballistic carbon nanotubes. Phys. Rev. Lett. **98**, 176802 (2007)
57. J. Cao, Q. Wang, M. Rolandi, H. Dai, Aharonov-Bohm interference and beating in single-walled carbon-nanotube interferometers. Phys. Rev. Lett. **93**, 216803 (2004)
58. C.L. Kane, E.J. Mele, Quantum spin hall effect in graphene. Phys. Rev. Lett. **95**, 226801 (2005)
59. S. Murakami, N. Nagaosa, S.-C. Zhang, Spin-hall insulator. Phys. Rev. Lett. **93**, 156804 (2004)
60. Y. Yao, F. Ye, X.-L. Qi, S.-C. Zhang, Z. Fang, Spin-orbit gap of graphene: First-principles calculations. Phys. Rev. B **75**, 041401 (R) (2007)
61. A. De Martino, R. Egger, K. Hallberg, C.A. Balseiro, Spin-orbit coupling and electron spin resonance theory for carbon nanotubes. Phys. Rev. Lett. **88** 206402 (2002); A. De Martino, R. Egger, F. Murphy-Armando, K. Hallberg, Spin–orbit coupling and electron spin resonance for interacting electrons in carbon nanotubes. J. Phys. Condens. Matter **16**, S1437 (2004)
62. T. Ando, Spin-Orbit Interaction in Carbon Nanotubes. J. Phys. Soc. Jpn. **69**, 1757 (2000)
63. D. Huertas-Hernando, F. Guinea, A. Brataas, Spin-orbit coupling in curved graphene, fullerenes, nanotubes, and nanotube caps. Phys. Rev. B **74**, 155426 (2006)
64. L. Chico, M.P. López-Sancho, M.C. Muñoz, Spin splitting induced by spin-orbit interaction in chiral nanotubes. Phys. Rev. Lett. **93**, 176402 (2004)
65. L. Chico, L.X. Benedict, S.G. Louie, M.L. Cohen, Quantum conductance of carbon nanotubes with defects. Phys. Rev. B **54**, 2600 (1996)
66. R. Landauer, IBM J. Res. Dev. **1**, 233 (1957); R. Landauer, Phil. Mag. **21**, 863 (1970)
67. W. Liang, M. Bockrath, D. Bozovic, J.H. Hafner, Tinkham, H. Park, Fabry-Perot interference in a nanotube electron waveguide. Nature (London) **411**, 665 (2001)
68. S. Frank, P. Poncharal, Z.L. Wang, W.A. De Heer, Carbon nanotube quantum resistors. Science **280**, 1744–1746 (1998)
69. S. Sanvito, Y.-K. Kwon, D. Tomànek, C.J. Lambert, Fractional quantum conductance in carbon nanotubes. Phys. Rev. Lett. **84**, 1974 (2000)
70. M.P. Anantram, Which nanowire couples better electrically to a metal contact: Armchair or zigzag nanotube? Appl. Phys. Lett. **78**, 2055 (2001)
71. N. Mingo, J. Han, Conductance of metallic carbon nanotubes dipped into metal. Phys. Rev. B **64**, 201401 (2001)
72. M.B. Nardelli, J.-L. Fattebert, J. Bernholc, *O*(*N*) real-space method for *ab initio* quantum transport calculations: Application to carbon nanotube–metal contacts. Phys. Rev. B **64**, 245423 (2001)
73. S. Dag, O. Gulseren, S. Ciraci, T. Yildirim, Electronic structure of the contact between carbon nanotube and metal electrodes. Appl. Phys. Lett. **83**, 3180 (2003)
74. J.J. Palacios, A.J. Perez-Jimenez, E. Louis, E. SanFabian, J.A. Verges, First-principles phase-coherent transport in metallic nanotubes with realistic contacts. Phys. Rev. Lett. **90**, 106801 (2003)
75. S. Okada, A. Oshiyama, Electronic structure of semiconducting nanotubes adsorbed on metal surfaces. Phys. Rev. Lett. **95**, 206804 (2005)
76. S.-H. Ke, W. Yang, H.U. Baranger, Nanotube-metal junctions: 2- and 3-terminal electrical transport. J. Chem. Phys. **124**, 181102 (2006)
77. N. Nemec, D. Tománek, G. Cuniberti, Contact dependence of carrier injection in carbon nanotubes: An *Ab Initio* study. Phys. Rev. Lett. **96**, 076802 (2006)
78. M.P. Anantram, Current-carrying capacity of carbon nanotubes. Phys. Rev. B **62**, R4837 (2000)
79. J. Kong, E. Yenilmez, T.W. Tombler, W. Kim, H.R.B. Laughlin, L. Liu, C.S. Jayanthi, S.Y. Wu, Quantum interference and ballistic transmission in nanotube electron waveguides. Phys. Rev. Lett. **87**, 106801 (2001)

80. D. Mann, A. Javey, J. Kong, Q. Wang, H. Dai, Ballistic transport in metallic nanotubes with reliable ohmic contacts. Nano Lett. **3**, 1541 (2003)
81. A. Javey, J. Guo, Q. Wang, M. Lundstrom, H.J. Dai, Ballistic carbon nanotube transistors. Nature (London) **424**, 654 (2003)
82. A. Javey, J. Guo, M. Paulsson, Q. Wang, D. Mann, Lundstrom, H. Dai, High-field quasiballistic transport in short carbon nanotubes. Phys. Rev. Lett. **92**, 106804 (2004)
83. P.J. de Pablo, C. Gomez-Navarro, J. Colchero, P.A. Serena, J. Gomez-Herrero, A. M. Baro, Nonlinear resistance versus length in single-walled carbon nanotubes. Phys. Rev. Lett. **88**, 036804 (2002)
84. T. Ando et al., *Mesoscopic Physics and Electronics* (Springer, Berlin, 1998)
85. S. Datta, *Electronic Transport in Mesoscopic Systems* (Cambridge University Press, Cambridge, 1995)
86. B.J. van Wees, L.P. Kouwenhoven, C.J.P.M. Harmans, J.G. Williamson, C.E. Timmering, M.E.I. Broekaart, C.T. Foxon, J.J. Harris, Observation of zero-dimensional states in a one-dimensional electron interferometer. Phys. Rev. Lett. **62**, 2523–2526 (1989)
87. M. Crommie, C.P. Lutz, D.M. Eigler, Confinement of Electrons to Quantum Corrals on a Metal Surface. Science **262**, 218–220 (1993)
88. Y. Ji et al., Science **290**, 779–783 (2000)
89. M.A. Topinka, B.J. LeRoy, S.E.J. Shaw, E.J. Heller, R.M. Westervelt, K.D. Maranowski, A.C. Gossard, Imaging coherent electron flow from a quantum point contact. Science **289**, 2323–2326 (2000)
90. H.C. Manoharan, C.P. Lutz, D.M. Eigler, Quantum mirages formed by coherent projection of electronic structure. Nature **403**, 512–515 (2000)
91. P. Debray, O.E. Raichev, P. Vasilopoulos, M. Rahman, R. Perrin, W.C. Mitchell, Ballistic electron transport in stubbed quantum waveguides: Experiment and theory. Phys. Rev. B **61**, 10950–10958 (2000)
92. C. Dekker, Carbon nanotubes as molecular quantum wires. Phys. Today **52**(5), 22–28 (1999)
93. C.T. White, T.N. Todorov, Carbon nanotubes as long ballistic conductors. Nature **393**, 240–242 (1998)
94. M. Buttiker, Y. Imry, R. Landauer, S. Pinhas, Generalized many-channel conductance formula with application to small rings. Phys. Rev. B **31**, 6207–6215 (1985)
95. M. Buttiker, Role of quantum coherence in series resistors. Phys. Rev. B **33**, 3020–3026 (1986)
96. M. Cahay, M. McLennan, S. Datta, Conductance of an array of elastic scatterers: A scattering-matrix approach. Phys. Rev. B **37**, 10125–10136 (1988)
97. M. Bockrath, D.H. Cobden, P.L. McEuen, N.G. Chopra, A. Zettl, A. Thess, R.E. Smalley, Single-electron transport in ropes of carbon nanotubes. Science **275**, 1922 (1997)
98. S.J. Tans, M.H. Devoret, R.J.A. Groeneveld, C. Dekker, Individual single-wall carbon nanotubes as quantum wires. Nature **386**, 474 (1997)
99. H.W.Ch. Postma, T. Teepen, Z. Yao, M. Grifoni, C. Dekker, Carbon nanotube single-electron transistors at room temperature. Science **293**, 76 (2001)
100. M.R. Buitelaar, A. Bachtold, T. Nussbaumer, M. Iqbal, C. Schönenberger, Multiwall carbon nanotubes as quantum dots. Phys. Rev. Lett. **88**, 156801 (2002)
101. L.P. Kouwenhoven, C. Marcus, Phys. World **11**, 35 (1998)
102. S. Tarucha, D.G. Austing, T. Honda, R.J. van der Hage, L.P. Kouwenhoven, Shell filling and spin effects in a few electron quantum dot. Phys. Rev. Lett. **77**, 3613 (1996)
103. T.H. Oosterkamp, J.W. Jansen, L.P. Kouwenhoven, D.G. Austing, T. Honda, S. Tarucha, Maximum-density droplet and charge redistributions in quantum dots at high magnetic fields. Phys. Rev. Lett. **82**, 2931 (1999)
104. C. Beenakker, Theory of Coulomb-blockade oscillations in the conductance of a quantum dot. Phys. Rev. B **44**, 1646 (1991)
105. O. Klein et al., Phase transitions in artificial atoms, in *Quantum Transport in Semiconductor Submicron Structures*, ed. by B. Kramer (Kluwer, Berlin, 1996)

106. L.P. Kouwenhoven, C.M. Marcus, P.L. McEuen, S. Tarucha, R.M. Westervelt, N.S. Wingreen, *Mesoscopic Electron Transport*, (Kluwer, Dordrecht, The Netherlands, 1997)
107. Y. Oreg, K. Byczuk, B.I. Halperin, Spin configurations of a carbon nanotube in a nonuniform external potential. Phys. Rev. Lett. **85**, 365 (2000)
108. D.H. Cobden, J. Nygard, Shell filling in closed single-wall carbon nanotube quantum dots. Phys. Rev. Lett. **89**, 46803 (2002)
109. W. Liang, M. Bockrath, H. Park, Shell filling and exchange coupling in metallic single-walled carbon nanotubes. Phys. Rev. Lett. **88**, 126801 (2002)
110. S.J. Tans, A.R.M. Verschueren, C. Dekker, Room-temperature transistor based on a single carbon nanotube. Nature **393**, 49 (1998)
111. D.H. Cobden, M. Bockrath, P.L. McEuen, A.G. Rinzler, R.E. Smalley, Spin splitting and even-odd effects in carbon nanotubes. Phys. Rev. Lett. **81**, 681 (1998)
112. P. Jarillo-Herrero, S. Sapmaz, C. Dekker, L.P. Kouwenhoven, H.S.J. van der Zant, Electron-hole symmetry in a semiconducting carbon nanotube quantum dot. Nature (London) **429**, 389 (2004)
113. P. Jarillo-Herrero, J. Kong, H.S.J. van der Zant, C. Dekker, L.P. Kouwenhoven, S. De Franceschi, Electronic transport spectroscopy of carbon nanotubes in a magnetic field. Phys. Rev. Lett. **94**, 156802 (2005)
114. S. Sapmaz, P. Jarillo-Herrero, Ya. M. Blanter, C. Dekker, H.S.J. van der Zant, Tunneling in suspended carbon nanotubes assisted by longitudinal phonons. Phys. Rev. Lett. **96**, 026801 (2006)
115. S. Bellucci, P. Onorato, Single-wall nanotubes: Atomiclike behavior and microscopic approach. Phys. Rev. B **71**, 075418 (2005)
116. J. Nygård, D.H. Cobden, P.E. Lindelof, Kondo physics in carbon nanotubes. Nature **408**, 342 (2000)
117. P. Jarillo-Herrero, J. Kong, H.S.J. van der Zant, C. Dekker, L.P. Kouwenhoven, S. De Franceschi, Orbital Kondo effect in carbon nanotubes. Nature **434**, 484 (2005)
118. B. Babić, T. Kontos, C. Schüonenberger, Kondo effect in carbon nanotubes at half filling. Phys. Rev. B **70**, 235419 (2004)
119. S. Moriyama, T. Fuse, M. Suzuki, Y. Aoyagi, K. Ishibashi, Four-electron shell structures and an tnteracting two-electron system in carbon-nanotube quantum dots. Phys. Rev. Lett. **94**, 186806 (2005)
120. S. Sapmaz, P. Jarillo-Herrero, J. Kong, C. Dekker, L.P. Kouwenhoven, H.S.J. van der Zant, Electronic excitation spectrum of metallic carbon nanotubes. Phys. Rev. B **71**, 153402 (2005)
121. A. Makarovski, L. An, J. Liu, G. Finkelstein, Evolution of transport regimes in carbon nanotube quantum dots. Phys. Rev. B **74**, 155431 (2006)
122. S. Moriyama, T. Fuse, T. Yamaguchi, K. Ishibashi, Phys. Rev. B **76**, 045102 (2007)
123. H. Ingerslev Jorgensen, K. Grove-Rasmussen, K.-Y. Wang, A.M. Blackburn, K. Flensberg, P.E. Lindelof, D.A. Williams, Nat. Phys. **4**, 536–539 (2008)
124. S. Tomonaga, Remarks on bloch's method of sound waves applied to many-fermion problems. Prog. Theor. Phys. **5**, 544 (1950)
125. J.M. Luttinger, An exactly soluble model of a many-fermion system. J. Math. Phys. **4**, 1154 (1963)
126. D.C. Mattis, E.H. Lieb, Exact solution of a many-fermion system and its associated boson field. J. Math. Phys. **6**, 304 (1965)
127. A. Yacoby, H.L. Stormer, N.S. Wingreen, L.N. Pfeiffer, K.W. Baldwin, K.W. West, Nonuniversal conductance quantization in quantum wires. Phys. Rev. Lett. **77**, 4612 (1996); O.M. Auslaender, A. Yacoby, R. de Picciotto, K.W. Baldwin, L.N. Pfeiffer, K.W. West, Experimental evidence for resonant tunneling in a Luttinger liquid. Phys. Rev. Lett. **84**, 1764 (2000)
128. S.J. Tans, M.H. Devoret, H. Dai, A. Thess, R.E. Smalley, L.J. Geerligs, C. Dekker, Individual single-wall carbon nanotubes as quantum wires. Nature **386**, 474 (1997)

129. Z. Yao, H.W.J. Postma, L. Balents, C. Dekker, Carbon nanotube intramolecular junctions. Nature **402**, 273 (1999)
130. C.L. Kane, M.P.A. Fisher, Experimental evidence for resonant tunneling in a Luttinger liquid. Phys. Rev. Lett. **68**, 1220 (1992)
131. C.L. Kane, M.P.A. Fisher, Resonant tunneling in an interacting one-dimensional electron gas. Phys. Rev. B **46**, R7268 (1992)
132. J. Sólyom, The Fermi gas model of one-dimensional conductors. Adv. Phys. **28**, 201 (1979)
133. J. Voit, One-dimensional Fermi liquids. Rep. Prog. Phys. **57**, 977 (1994)
134. H.J. Schulz, in *Proceedings of Les Houches Summer School LXI*, ed. by E. Akkermans, G. Montambaux, J. Pichard, J. Zinn-Justin (Elsevier, Amsterdam, 1995) p. 533
135. F.D.M. Haldane, Effective harmonic-fluid approach to low-energy properties of one-dimensional quantum fluids. Phys. Rev. Lett. **47**, 1840 (1981)
136. H.J. Schulz, G. Cuniberti, P. Pieri, in *Field Theories for Low-Dimensional Condensed Matter Systems*, ed. by G. Morandi (Springer, Berlin, 2000)
137. T. Giamarchi, *Quantum Physics in One Dimension* (Oxford, Clarendon, 2004)
138. W. Häusler, L. Kecke, A.H. MacDonald, Tomonaga-Luttinger parameters for quantum wires. Phys. Rev. B **65**, 085104 (2002)
139. R. Egger, A.O. Gogolin, Correlated transport and non-Fermi-liquid behavior in single-wall carbon nanotubes. Eur. Phys. J. B **3**, 281 (1998)
140. R. Egger, A.O. Gogolin, Effective low-energy theory for correlated carbon nanotubes. Phys. Rev. Lett. **79**, 5082 (1997)
141. R. Egger, A. Bachtold, M. Fuhrer, M. Bockrath, D. Cobden, P. McEuen, in *Interacting Electrons in Nanostructures*, ed. by R. Haug, H. Schoeller. Lecture Notes in Physics, vol 579 (Springer, Berlin, 2001)
142. C. Kane, L. Balents, M.P.A. Fisher, Coulomb interactions and mesoscopic effects in carbon nanotubes. Phys. Rev. Lett. **79**, 5086 (1997)
143. R. Egger, Luttinger liquid behavior in multiwall carbon nanotubes. Phys. Rev. Lett. **83**, 5547 (1999)
144. R. Egger, A.O. Gogolin, Bulk and boundary zero-bias anomaly in multiwall carbon nanotubes. Phys. Rev. Lett. **87**, 066401 (2001)
145. V. Derycke, R. Martel, J. Appenzeller, Ph. Avouris, Controlling doping and carrier injection in carbon nanotube transistors. Appl. Phys. Lett. **80**, 2773 (2002)
146. P.G. Collins, K. Bradley, M. Ishigami, A. Zettl, Extreme oxygen sensitivity of electronic properties of carbon nanotubes. Science, **287**, 1801 (2000)
147. G.U. Sumanasekera, C.K.W. Adu, S. Fang, P.C. Eklund, Effects of gas adsorption and collisions on electrical transport in single-walled carbon nanotubes. Phys. Rev. Lett. **85**, 1096 (2000)
148. K. Bradley, S.-H. Jhi, P.G. Collins, J. Hone, M.L. Cohen, S.G. Louie, A. Zettl, Is the intrinsic thermoelectric power of carbon nanotubes positive? Phys. Rev. Lett. **85**, 4361 (2000)
149. S.-H. Jhi, S.G. Louie, M.L. Cohen, Electronic properties of oxidized carbon nanotubes. Phys. Rev. Lett. **85**, 1710 (2000)
150. M. Bockrath, J. Hone, A. Zettl, P.L. McEuen, A.G. Rinzler, R.E. Smalley, Chemical doping of individual semiconducting carbon-nanotube ropes. Phys. Rev. B **61**, R10606 (2000)
151. C. Zhou, J. Kong, E. Yenilmez, H. Dai, Modulated chemical doping of individual carbon nanotubes. Science **290**, 1552 (2000)
152. M. Krüger, M.R. Buitelaar, T. Nussbaumer, C. Schönenberger, L. Forró, The electrochemical nanotube field-effect transistor. Appl. Phys. Lett. **78**, 1291 (2001)
153. A. Bachtold, M. de Jonge, K. Grove-Rasmussen, P.L. McEuen, M. Buitelaar, C. Schönenberger, Suppression of tunneling into multiwall carbon nanotubes. Phys. Rev. Lett. **87**, 166801 (2001)
154. S. Bellucci, in *Path Integrals from peV and TevV*, ed. by R. Casalbuoni et al. (World Scientific, Singapore, 1999) p. 363
155. S. Bellucci, J. González, Crossover from marginal Fermi liquid to Luttinger liquid behavior in carbon nanotubes. Phys. Rev. B **64**, 201106 (2001)

156. S. Bellucci, J. González, P. Onorato, Large N effects and renormalization of the long-range Coulomb interaction in carbon nanotubes. Nucl. Phys. B **663**, (2003)
157. S. Bellucci, P. Onorato, Magnetic field effects and renormalization of the long-range Coulomb interaction in Carbon Nanotubes. Ann. Phys. **321**, 934 (2006)
158. S. Bellucci, J. González, P. Onorato, Doping- and geometry-dependent suppression of tunneling in carbon nanotubes. Phys. Rev. B **69**, 085404 (2004)
159. R. Egger, H. Grabert, Electroneutrality and the Friedel sum rule in a Luttinger liquid. Phys. Rev. Lett. **79**, 3463 (1997)
160. S. Xu, J. Cao, C.C. Miller, D.A. Mantell, R.J.D. Miller, Y. Gao, Energy dependence of electron lifetime in graphite observed with femtosecond photoemission spectroscopy. Phys. Rev. Lett. **76**, 483 (1996)
161. C. Castellani, C. Di Castro, W. Metzner, Dimensional crossover from Fermi to Luttinger liquid. Phys. Rev. Lett. **72**, 316 (1994)
162. S. Bellucci, J. González, On the Coulomb interaction in chiral-invariant one-dimensional electron systems. Eur. Phys. J. B **18**, 3 (2000)
163. P.W. Anderson, *The Theory of Superconductivity in the High-$T_c$ Cuprates* (Princeton University Press, Princeton, 1997)
164. D.W. Wang, A.J. Millis, S. Das Sarma, Coulomb Luttinger liquid. Phys. Rev. B **64**, 193307 (2001)
165. M. Bockrath, D.H. Cobden, J. Lu, A.G. Rinzler, R.E. Smalley, L. Balents, P.L. McEuen, Luttinger liquid behavior in carbon nanotubes. Nature (London) **397**, 598 (1999)
166. J.E. Fischer, H. Dai, A. Thess, R. Lee, N.M. Hanjani, D.L. Dehaas, R.E. Smalley, Metallic resistivity in crystalline ropes of single-wall carbon nanotubes. Phys. Rev. B **55**, R4921 (1997)
167. B. Gao, A. Komnik, R. Egger, D.C. Glattli, A. Bachtold, Evidence for Luttinger-liquid behavior in crossed metallic single-wall nanotubes. Phys. Rev. Lett. **92**, 216804 (2004)
168. H. Ishii et al., Direct observation of Tomonaga–Luttinger-liquid state in carbon nanotubes at low temperatures. Nature (London) **426**, 540 (2003)
169. P.M. Singer, P. Wzietek, H. Alloul, F. Simon, H. Kuzmany, NMR evidence for gapped spin excitations in metallic carbon nanotubes. Phys. Rev. Lett. **95**, 236403 12 (2005)
170. A. Kanda, K. Tsukagoshi, Y. Aoyagi, Y. Ootuka, Gate-voltage dependence of zero-bias anomalies in multiwall carbon nanotubes. Phys. Rev. Lett. **92**, 36801 (2004)
171. S. Bellucci, P. Onorato, Magnetic field effects on low dimensional electron systems: Luttinger liquid behaviour in a quantum wire. Eur. Phys. J. B **45**, 87 (2005)
172. L. Chico, V.H. Crespi, L.X. Benedict, S.G. Louie, M.L. Cohen, Pure carbon nanoscale devices: Nanotube heterojunctions. Phys. Rev. Lett. **76**, 971–974 (1996)
173. Ph. Lambin, A. Fonseca, J.P. Vigneron, J.B. Nagy, A.A. Lucas, Structural and electronic properties of bent carbon nanotubes. Chem. Phys. Lett. **245**, 85–89 (1995)
174. R. Saito, G. Dresselhaus, M.S. Dresselhaus, Tunneling conductance of connected carbon nanotubes. Phys. Rev. B **53**, 2044–2050 (1996)
175. J.-C. Charlier, T.W. Ebbesen, Ph. Lambin, Structural and electronic properties of pentagon-heptagon pair defects in carbon nanotubes. Phys. Rev. B **53**, 11108–11113 (1996)
176. M. Menon, D. Srivastava, Carbon nanotube "T junctions": Nanoscale metal-semiconductor-metal contact devices. Phys. Rev. Lett. **79**, 4453–4456 (1997)
177. L. Chico, M.P. López Sancho, M.C. Muñoz, Carbon-nanotube-based quantum dot. Phys. Rev. Lett. **81**, 1278–1281 (1998)
178. H.W.Ch. Postma, T. Teepen, Z. Yao, M. Grifoni, C. Dekker, Carbon nanotube single-electron transistors at room temperature. Science **293**, 76 (2001)
179. D. Bozovic, M. Bockrath, J.H. Hafner, C. M. Lieber, H. Park, M. Tinkham, Electronic properties of mechanically induced kinks in single-walled carbon nanotubes. Appl. Phys. Lett. **78**, 3693 (2001)
180. M. Sassetti, F. Napoli, U. Weiss, Coherent transport of charge through a double barrier in a Luttinger liquid. Phys. Rev. B **52**, 11213 (1995)

181. A. Furusaki, Resonant tunneling through a quantum dot weakly coupled to quantum wires or quantum Hall edge states. Phys. Rev. B **57**, 7141 (1998)
182. A. Braggio, M. Grifoni, M. Sassetti, F. Napoli, Plasmon and charge quantization effects in a double-barrier quantum wire. Europhys. Lett. **50**, 236 (2000)
183. M. Thorwart, M. Grifoni, G. Cuniberti, H.W.Ch. Postma, C. Dekker, Correlated tunneling in intramolecular carbon nanotube quantum dots. Phys. Rev. Lett. **89**, 196402 (2002)
184. Yu.V. Nazarov, L.I. Glazman, Resonant tunneling of interacting electrons in a one-dimensional wire. Phys. Rev. Lett. **91**, 126804 (2003)
185. D.G. Polyakov, I.V. Gornyi, Transport of interacting electrons through a double barrier in quantum wires. Phys. Rev. B **68**, 035421 (2003)
186. A. Komnik, A.O. Gogolin, Resonant tunneling between Luttinger liquids: A solvable case. Phys. Rev. Lett. **90**, 246403 (2003)
187. S. Hügle, R. Egger, Resonant tunneling in a Luttinger liquid for arbitrary barrier transmission. Europhys. Europhys. Lett. **66**, 565 (2004)
188. A. Furusaki, N. Nagaosa, Resonant tunneling in a Luttinger liquid. Phys. Rev. B **47**, 3827 (1993)
189. V. Meden, T. Enss, S. Andergassen, W. Metzner, K. Schönhammer, Correlation effects on resonant tunneling in one-dimensional quantum wires. Phys. Rev. B **71**, 041302(R) (2005)
190. H.J. Choi, J. Ihm, S.G. Louie, M.L. Cohen, Defects, quasibound states, and quantum conductance in metallic carbon nanotubes. Phys. Rev. Lett. **84**, 2917 (2000)
191. S. Bellucci, J. González, P. Onorato, Crossover from Luttinger liquid to Coulomb blockade regime in carbon nanotubes. Phys. Rev. Lett. **95**, 186403 (2005)
192. S. Bellucci, J. Gonzalez, P. Onorato, E. Perfetto, Modulation of Luttinger liquid exponents in multi-walled carbon nanotubes. Phys. Rev. B **74**, 045427 (2006)
193. D. Goldhaber-Gordon, H. Shtrikman, D. Mahalu, D. Abusch-Magder, U. Meirav, M.A. Kastner, Kondo effect in a single-electron transistor. Nature **391**, 156 (1998)
194. J. Nygard, D.H. Cobden, P.E. Lindelof, Kondo physics in carbon nanotubes. Nature **408**, 342 (2000)
195. J. Paaske, A. Rosch, P. Wolfle, N. Mason, C.M. Marcus, J. Nygard, Non-equilibrium singlet-triplet Kondo effect in carbon nanotubes. Nat. Phys. **2**, 460 (2006)
196. P. Jarillo-Herrero, J. Kong, H.S.J. van der Zant, C. Dekker, L.P. Kouwenhoven, S. De Franceschi, Orbital Kondo effect in carbon nanotubes. Nature **434**, 484 (2005)
197. A. Makarovski, J. Liu, G. Finkelstein, Evolution of transport regimes in carbon nanotube quantum dots. Phys. Rev. Lett. **99**, 066801 (2007)
198. J.V. Holm, H.I. Jorgensen, K. Grove-Rasmussen, J. Paaske, K. Flensberg, P.E. Lindelof, Gate-dependent tunneling-induced level shifts observed in carbon nanotube quantum dots. Phys. Rev. B **77**, 161406 (2008)
199. N.D. Mermin, H. Wagner, Absence of ferromagnetism or antiferromagnetism in one- or two-dimensional isotropic Heisenberg models. Phys. Rev. Lett. **17**, 1133 (1966)
200. Z.K. Tang, L. Zhang, N. Wang, X.X. Zhang, G.H. Wen et al., Superconductivity in 4 Angstrom single-walled carbon nanotubes. Science **292**, 2462 (2001)
201. I. Takesue, J. Haruyama, N. Kobayashi, S. Chiashi, S. Maruyama, T. Sugai, H. Shinohara, Superconductivity in entirely end-bonded multiwalled carbon nanotubes. Phys. Rev. Lett. **96**, 057001 (2006)
202. A.Yu. Kasumov, R. Deblock, M. Kociak, B. Reulet, H. Bouchiat, I.I. Khodos, Yu.B. Gorbatov, V.T. Volkov, C. Journet, M. Burghard, Supercurrent through single-walled carbon nanotubes. Science **284**, 1508 (1999)
203. A.F. Mopurgo, J. Kong, C.M. Marcus, H. Dai, Gate-controlled superconducting proximity effect in carbon nanotubes. Science **286**, 263 (1999)
204. M. Kociak, A.Yu. Kasumov, S. Guéron, B. Reulet, I.I. Khodos, Yu.B. Gorbatov, V.T. Volkov, L. Vaccarini, H. Bouchiat, Superconductivity in ropes of single-walled carbon nanotubes. Phys. Rev. Lett. **86**, 2416 (2001)

205. A.A. Kasumov, M. Kociak, M. Ferrier, R. Deblock, S. Guéron, B. Reulet, I. Khodos, O. Stéphan, H. Bouchiat, Quantum transport through carbon nanotubes: Proximity-induced and intrinsic superconductivity. Phys. Rev. B **68**, 214521 (2003)
206. M.R. Buitelaar, W. Belzig, T. Nussbaumer, B. Babic, C. Bruder, C. Schönenberger, Multiple Andreev reflections in a carbon nanotube quantum. Phys. Rev. Lett. **91**, 057005 (2003); E. Vecino, M.R. Buitelaar, A. Martýn-Rodero, C. Schönenberger, A.L. Yeyati, Conductance properties of nanotubes coupled to superconducting leads: signatures of Andreev states dynamics. Solid State Commun. **131**, 625 (2004)
207. J. Haruyama, A. Tokita, N. Kobayashi, M. Nomura, S. Miyadai et al., End-bonding multiwalled carbon nanotubes in alumina templates: Superconducting proximity effect. Appl. Phys. Lett. **84**, 4714 (2004)
208. T. Tsuneta, L. Lechner, P.J. Hakonen, Gate-controlled superconductivity in a diffusive multiwalled carbon nanotube. Phys. Rev. Lett. **98**, 087002 (2007)
209. N. Murata, J. Haruyama, Y. Ueda, M. Matsudaira, H. Karino, Y. Yagi, E. Einarsson, S. Chiashi, S. Maruyama, T. Sugai, N. Kishi, H. Shinohara, Meissner effect in honeycomb arrays of multiwalled carbon nanotubes. Phys. Rev. B **76**, 245424 (2007)
210. R.E. Peierls, *Quantum Theory of Solids* (Clarendon, Oxford, 1955)
211. M. Ferrier, A. De Martino, A. Kasumov, S. Gueron, M. Kociak, R. Egger, H. Bouchiat, Superconductivity in ropes of carbon nanotubes. Solid State Commun. **131**, 615 (2004)
212. A. De Martino, R. Egger, Effective low-energy theory of superconductivity in carbon nanotube ropes. Phys. Rev. B **70**, 014508 (2004)
213. J. González, Consistency of superconducting correlations with one-dimensional electron interactions in carbon nanotubes. Phys. Rev. Lett. **87**, 136401 (2001)
214. J. González, Microscopic model of superconductivity in carbon nanotubes. Phys. Rev. Lett. **88**, 076403 (2002)
215. A.A. Maarouf, C.L. Kane, E.J. Mele, Electronic structure of carbon nanotube ropes. Phys. Rev. B **61**, 11156 (2000)
216. H.J. Schulz, in *Correlated Electron Systems*, ed. by V.J. Emery, vol 9 (World Scientific, Singapore, 1993)
217. J. González, Superconductivity in carbon nanotube ropes. Phys. Rev. B **67**, 014528 (2003)
218. J.V. Alvarez, J. González, Insulating, superconducting, and large-compressibility phases in nanotube ropes. Phys. Rev. Lett. **91**, 076401 (2003)
219. J. González, Current instability and diamagnetism in small-diameter carbon nanotubes. Phys. Rev. B **72**, 073403 (2005)
220. K.-P. Bohnen, R. Heid, H.J. Liu, C.T. Chan, Lattice dynamics and electron-phonon interaction in (3,3) carbon nanotubes. Phys. Rev. Lett. **93**, 245501 (2004)
221. D. Connétable, G.-M. Rignanese, J.-C. Charlier, X. Blase, Room temperature Peierls distortion in small diameter nanotubes. Phys. Rev. Lett. **94**, 015503, (2005)
222. E. Perfetto, J. González, Theory of superconductivity in multiwalled carbon nanotubes. Phys. Rev. B **74**, 201403 (2006)
223. K. Kamide, T. Kimura, M. Nishida, S. Kurihara, Singlet superconductivity phase in carbon nanotubes. Phys. Rev. B **68**, 024506 (2003)
224. D. Carpentier, E. Orignac, Superconducting instability in three-band metallic nanotubes. Phys. Rev. B **74**, 085409 (2006)
225. K. Sasaki, J. Jiang, R. Saito, S. Onari, Y. Tanaka, Theory of superconductivity of carbon nanotubes and graphene. J. Phys. Soc. Jpn. **76**, 033702 (2007)
226. S. Bellucci, M. Cini, P. Onorato, E. Perfetto, Suppression of electron electron repulsion and superconductivity in ultra small carbon nanotubes. J. Phys. Condens. Matter **18**, S2115 (2006)
227. S. Bellucci, M. Cini, P. Onorato, E. Perfetto, Theoretical approach to electronic screening and correlated superconductivity in carbon nanotubes. Phys. Rev. B **75**, 014523 (2007)

228. E. Perfetto, G. Stefanucci, M. Cini, $W$=0 pairing in ($N$,$N$) carbon nanotubes away from half filling. Phys. Rev. B **66**, 165434 (2002)
229. E. Perfetto, G. Stefanucci, M. Cini, On-site repulsion as the origin of pairing in carbonnanotubes and intercalated graphite. Eur. Phys. J. B **30**, 139 (2002)
230. S. Bellucci, M. Cini, P. Onorato, E. Perfetto, Influence of dimensionality on superconductivity in carbon nanotubes. J. Phys. Condens. Matter **19**, 395016 (2007)

http://www.springer.com/978-3-642-15777-6

Physical Properties of Ceramic and Carbon Nanoscale Structures
The INFN Lectures, Vol. II
Bellucci, S. (Ed.)
2011, XIV, 198 p., Hardcover
ISBN: 978-3-642-15777-6